Plant Ecology & Diversity, 2013
http://dx.doi.org/10.1080/17550874.2013.795629

Gap formation and carbon cycling in the Brazilian Amazon: measurement using high-resolution optical remote sensing and studies in large forest plots

Fernando D.B. Espírito-Santo[a,b]*, Michael M. Keller[a,c,d], Ernst Linder[e], Raimundo C. Oliveira Junior[f], Cleuton Pereira[f] and Cleber G. Oliveira[g]

[a]*Institute for the Study of Earth, Oceans and Space, Morse Hall, University of New Hampshire, Durham, NH, USA;* [b]*Jet Propulsion Laboratory, Radar Science and Engineering Section, Pasadena, CA, USA;* [c]*USDA Forest Service, International Institute of Tropical Forestry, San Juan, Puerto Rico;* [d]*Embrapa Monitoramento por Satélite, Av. Soldado Passarinho 303, Fazenda Chapadão, Campinas, Brasil;* [e]*Department of Mathematics and Statistics, University of New Hampshire, Durham, NH, USA;* [f]*EMBRAPA Amazônia Oriental, Santarém, Brasil;* [g]*Instituto Nacional de Pesquisas Espaciais, São José dos Campos, Brasil*

(*Received 28 February 2013; final version received 10 April 2013*)

Background: The dynamics of gaps plays a role in the regimes of tree mortality, production of coarse woody debris (CWD) and the variability of light in the forest understory.
Aims: To quantify the area affected by, and the carbon fluxes associated with, natural gap-phase disturbances in a tropical lowland evergreen rain forest by use of ground measurements and high-resolution satellite images.
Methods: We surveyed two large forest inventory plots of 114 and 53 ha of the Tapajós National Forest (TNF) in the Brazilian Amazon during 2008 and 2009, respectively. We mapped all gaps and collected data on light availability, CWD stocks and tree mortality in the field. Gap location, canopy openness (CO) and leaf area index (LAI) estimated in the field were compared with two IKONOS–2 high-resolution satellite images acquired at approximately the time of the field measurements.
Results: In the two large plots (167 ha total area) we found 96 gaps. The gaps represented 1.42% of the total area and gaps <1-year-old accounted for 0.81% of the plot area. In TNF, the production of CWD in recent gaps was 0.76 Mg C ha^{-1} year^{-1} and the mean tree mortality was 2.38 stems ha^{-1} year^{-1}. The area of gaps estimated using thresholds of light intensity measured by remote sensing optical instruments was twice as large as the gap areas measured on the ground. We found no significant correlation between spectral remote sensing images and CO or LAI, probably due to the high degree of shadow in the high-resolution satellite images.
Conclusions: We present the first statistics of CWD production based on gap size in the tropical forest literature. Tree mortality and CWD flux and the forest floor light environment were closely related to gap area. However, less than 30% of the annual tree mortality and CWD flux was associated with gaps, and gaps were difficult to detect using remote sensing methods because of the high proportion of shadow in the images. These results highlight the need for permanent plots in long-term carbon studies.

Keywords: Amazon; canopy opening; coarse wood debris gaps; leaf area index natural disturbances; remote sensing; tropical forest; IKONOS

Introduction

The formation of gaps in tropical forests continually reshapes forest structure (Whitmore 1989; Brokaw and Scheiner 1989) and is a mechanism for the maintenance of biodiversity (Denslow 1987; Hubbell et al. 1999). Gaps produced by tree falls and subsequent regrowth (Brokaw 1982; Uhl et al. 1988) create the characteristic patchwork structure of old growth tropical forests and are important for forest dynamics and carbon cycling (Shugart 1984). The impact of gap formation on tropical forest carbon cycling can be measured by tree mortality at the plot level (Phillips et al. 1998; Clark et al. 2000; Clark and Clark 2000), by measurement of the stocks of coarse woody debris (CWD) (Delaney et al. 1997; Clark et al. 2002; Baker et al. 2004; Chambers et al. 2004; Keller et al. 2004; Palace et al. 2007), or more rarely by measurement of the CWD flux – input of new tree or branch falls to the CWD pool (Palace et al. 2008).

Few studies of canopy dynamics have attempted to map the distribution of small frequently occurring gaps in tropical forest (Hubbell et al. 1999) and few, if any, have attempted to relate the occurrence of natural disturbances to production of CWD, a large pool of ecosystem carbon (Denslow 1987; Clark et al. 2002; Chambers et al. 2004; Keller et al. 2004; Rice et al. 2004; Palace et al. 2007) and nutrients (Clark et al. 2002). We are unaware of any study in the tropical forest literature that estimates the relationship between the geometry of gaps (e.g. area, perimeter) and the amount of CWD produced by natural tree mortality or branch fall disturbances. The relationship between disturbed area and its biophysical consequences (e.g. tree mortality or CWD) is valuable for the quantification of the effects of disturbance on carbon cycling in forest ecosystems (Turner 2010). Passive optical remote sensing provides information that is mainly relevant to quantification of the area of disturbance in tropical forests. The

*Corresponding author. Email: f.delbon@gmail.com

intensity of such events in terms of carbon fluxes can only be estimated by empirical calibration between disturbed area and field data.

Forest disturbances caused by tree-falls and/or branch-falls can be described either in terms of the number of dead trees or with regard to the sizes and rates of production of canopy gaps (van der Meer and Bongers 1996). Physically, gaps have been defined in many ways but are generally divided into two categories, exemplified by the Brokaw (1982) and Runkle (1981) gap definitions. Brokaw (1982) defined gap formation at the upper level of the top canopy wherein gaps are vertical holes, defined by a plumb line extending from the foliage at the gap edge down to a selected height above ground (e.g. 2 m) (Brokaw 1982). Runkle (1981) defined gaps at the ground level as the area under a canopy opening extending to the base of the surrounding canopy trees defined by a minimum trunk diameter of 20 cm and height of 10 m (Runkle 1981). The definition of Runkle (1981) includes areas directly and indirectly affected by the canopy opening by light enhancement at the forest floor. Depending on the definition used, the area measured can easily vary by a factor of two. This makes quantitative interpretation of tree-fall disturbance regimes impossible unless accompanied by a clear gap definition (Brokaw 1982). Although gaps can be detected and mapped using these definitions, Lieberman and Lieberman (1989) have argued that the dichotomy of forest environments into gap and non-gap is both unrealistic and difficult to implement with rigour and consistency. Instead they argue that the forest light environments should be treated as a continuum. The spatial distribution of light environments caused by disturbance regimes reshapes canopy biophysical proprieties (e.g. leaf area index), canopy functions (e.g. photosynthesis) and forest dynamics (e.g. forest growth and mortality) (Denslow 1987).

Remote sensing provides a means of analysing gap formation at multiple scales. Data from high spatial resolution sensors such as IKONOS (GeoEye Inc.) have been used in tropical forests to measure tree crown sizes (Asner et al. 2002; Clark et al. 2004a; Barbier et al. 2010), to estimate mortality in dominant trees (Clark et al. 2004b), to determine the effects of selective logging (Read et al. 2003) and in other ecological applications (Clark et al. 2004a, 2004b). However, high-resolution images have rarely been used to estimate gap formation or natural disturbances in tropical forests, with the exception of demographic studies of emergent tree mortality in Costa Rica (Read et al. 2003; Clark et al. 2004a, 2004b).

The aim of the present study was to improve the quantification of the area affected by and the carbon cycle effects of natural gap-phase disturbances in a tropical evergreen lowland rain forest in the Brazilian Amazon. Working in large plots we linked gap formation with carbon cycling through analysis of the CWD inside the gaps and linked measurement of gap area with the quantity of CWD. By using ground-based optical instruments we quantified light penetration in the plot areas to estimate the effects of gap disturbances. We investigated how remote sensing could be used to estimate tree-fall and/or branch-fall disturbances and attempted to detect small disturbances using high-resolution satellite images and spectral analysis. We compared the detection of gaps using high-resolution remote sensing and detailed ground-based forest survey, supplemented by instrumental measurements of light penetration.

Materials and methods

Study area and large forest survey plots

The study was conducted in an area of the Tapajós National Forest (TNF; 2° 32′ and 4° 18′ S; 54° 30′ and 55° 29′ W), Pará, Brazil (Figure 1(a)–(c)). The tropical moist forest in the TNF experiences a wet season from January to May, with 70% of the annual precipitation falling during this period. Forest structure and biogeochemical characteristics of this forest have been described elsewhere (Silver et al. 2000; Keller et al. 2001). The total live above-ground biomass (including vines and epiphytes) has been estimated at ca. 282 Mg ha^{-1} (Keller et al. 2001) and above-ground necromass at ca. 85 Mg ha^{-1} (Palace et al. 2001).

We installed and surveyed two large forest inventory plots of 114 and 53 ha in an unmanaged forest area of the TNF (Figure 1(a)–(g)). The 114 ha plot was installed between August and September 2008 and the 53 ha plot between August and October 2009. We made measurements of the following forest disturbance variables: (1) mode of gap formation; (2) light environment over the gap areas; (3) light environment of the large plot surveys; and (4) coarse woody debris inside the gap areas. Ground measurements were used to calibrate the high-resolution satellite images (IKONOS–2) acquired within two months of the field campaigns.

Mode of gap formation

We mapped all gaps in both large plots using the gap definition of Runkle (1981): opened canopy, extending to the base of surrounding trees of $>$20 cm diameter at breast height (DBH) and 10 m in height, and including areas directly or indirectly affected by the canopy opening. We collected data on light availability (canopy openness) and estimated leaf area index (LAI) for the whole large plot area. For each gap we collected the following data: (1) mode of formation, (2) disturbance age, (3) gap area and perimeter at the ground level, (4) proportion of canopy openness (CO), and (5) LAI. We defined the modes of gap formation based on the type of disturbance: (a) partial or complete crown-fall (from either live or dead standing trees), (b) snapped bole-fall, and (c) uprooted tree-fall. We classified all gaps into two age classes: (i) recent disturbances, $<$1 year; and (b) old disturbances, $\geq$1 year. For each gap identified in the field we collected a central Global Positioning System

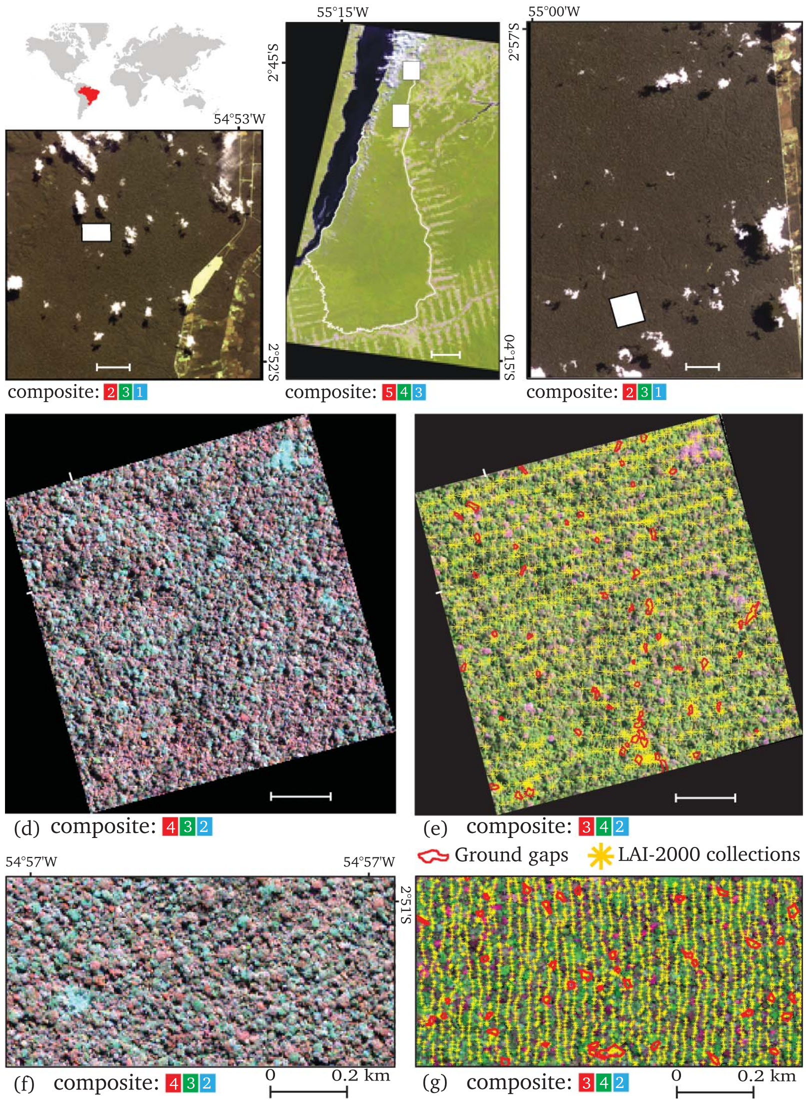

Figure 1. Survey of ground gaps (red lines) and leaf area index (LAI; yellow dots) collected in large forest inventory plots in the Tapajós National Forest, Pará, Brazil (TNF). (a) 53 ha plot (white box) overlapped in an IKONOS-2 image acquired 8 August 2009. (b) Location of TNF in a TM Landsat acquired 30 July 2001 and the overlapped IKONOS-2 images. (c) 114 ha plot (white box) overlapped the IKONOS-2 image of 23 June 2008. (d) Forest canopy details of the 114 ha plot survey in the 4 m multispectral IKONOS-2 bands. (e) Ground collections of gaps (n = 55, Runkle's gap definition), hemispherical photos (n = 110, two photos per gap) and biophysical data of canopy openness (CO) and LAI collected with LAI-2000 plant canopy analyzer (n = 980) in 114 ha plot overlapped in a 4 m multispectral IKONOS-2 image. (f) Forest canopy details of the 53 ha plot survey in IKONOS-2 multispectral images. (g) Ground collections of gaps (n = 41), hemispherical photos (n = 82), LAI-2000 (n = 2315) in 53 ha overlapped in a visible multispectral band composition of IKONOS-2 images. Colour compositions of Landsat image at full-width wavelength for the three bands are: (3) red 0.63–0.69 μm; (4) near-IR 0.76–0.90 μm; and (5) mid-IR 1.55–1.75 μm. For the IKONOS–2 image the wavelength bands are: (2) green 0.51–0.60 μm; (3) red 0.63–0.70 μm; and (4) NIR 0.76–0.85 μm.

(GPS) coordinate using an average of 53 way-points (collection time about 2 min) using a GPS receiver (Garmin GPSMAP 76CSx). From the centre of each gap we measured the distance and the azimuth of each large tree (DBH >20 cm) along the gap edge using a laser rangefinder (Impulse–200LR, Laser Technology Corp.) and a magnetic compass corrected for magnetic declination (NOAA 2010). We delimited each gap with at least eight edge vertices. We estimated the recurrence interval (turnover) of gaps using the area of tree-fall <1-year-old, in the form of total area studied divided by gap area formed per year.

Light environments over the gaps areas

We quantified the CO and LAI for each gap using indirect measurements of hemispherical photographs. Two photos were taken at the centre of each gap, 1.5 m above the forest floor, with a colour digital camera, Nikon Coolpix 950, and FC–E8 fish-eye lens (180° field of view). The photographs were taken using a tripod (1.6 m above the ground) and collected in the early morning, late afternoon, or after clouds had eclipsed the sun (Rich 1989). The lens was facing skywards and the camera body was oriented magnetic north, allowing superposition of solar tracks. The CO of the photos was analysed using the image-processing software, Gap Light Analyzer (GLA), version 2 (Frazer et al. 1999). Considering the colour blurring or chromatic aberration associated with digital cameras (Frazer et al. 2001), we used an automatic threshold algorithm for hemispherical canopy photographs based on edge detection (Nobis and Hunziker 2005) to separate canopy and sky elements, producing a binary black and white image. The automatic threshold was applied to all images using the edge value mode (Nobis and Hunziker 2005). All photographs were saved in grey scale (BMP format) and CO was extracted following Frazer et al. (1999). In order to reduce the artefacts associated with image processing and sky conditions, we averaged the CO of the two photographs collected in each gap.

Light environments of the large forest survey plots

We examined the spatial distribution of sky opening for the whole plots using diffuse non-interceptance (DIFN) canopy and LAI estimates produced by the LAI–2000 (LI–COR Inc. 1992) plant canopy analyser (PCA). We estimated the CO and LAI in both plots, where the CO represented values of DIFN collected with LAI–2000 PCA at a height of 1.5 m. We used two inter-calibrated LAI–2000 PCA sensors; one sensor was installed in an open area without obstruction (above the unit) to measure the instantaneous diffuse solar radiation, and the other was used to collect the data along the forest transects (below the unit) (Welles and Norman 1991). Both sensors were oriented in the same direction, pointing away from the sun using a compass. The measurements were carried out in the early morning (5:30 am) or late afternoon (5:30 pm) to minimise the incidence of direct sun on the sensor. We omitted one of the five LAI–2000 sensor readers (lens No 5) due to the large variability in measurements introduced by that lens.

In the 114 ha plot, the LAI and CO measurements were made along 21 transects of 1 km length, at a separation of 50 m. Along each 1 km line we collected data from the LAI–2000 and GPS coordinates at points separated by ca. 15 m along the transect, to produce a grid of CO and LAI data with ca. 15 m × 50 m spatial resolution. We used this data to map all gaps by light availability near the forest floor. For the 53 ha plot we collected data on light availability more intensively. In this plot measurements were made along 41 transects of 0.5 km length with a separation between lines of 25 m (double the density of that in the 114 ha plot). When the gaps occurred between the lines, we explicitly collected ground data of LAI–2000 at the centre and edge of these gaps in order to obtain the maximum spatial variance of CO and LAI. In total, 21 days were needed in each plot to measure the DIFN by LAI–2000 PCA due to the high density of data collection inside these large grids.

Of the 980 measurements of DIFN data for the 114 ha plot (Figure 1(e)), only 731 ground data were used for the geostatistical analysis of CO and LAI. We eliminated 249 points in which DIFN = 0 where inspection of the data indicated that the LAI–2000 devices had failed and produced consecutive zero values. These 249 samples represented a set of consecutive measurements (1.5 transect lines) and a few points where DIFN = 0 in the darkest regions of the plot. Along these 1.5 transect lines we had only the small and old gaps (>1-year-old) that had a minor impact on our analysis of light variability in this plot. In the 53 ha plot 2315 measurements were collected (Figure 1(g)).

In order to investigate the relationship between forest disturbance detected by ground measurements of LAI–2000 and remote sensing, the DIFN surveys of CO and LAI in the 114 ha and 53 ha plots were interpolated at the spatial resolution of the high-resolution remote sensing images (ca. 4 m). CO estimates the percentage of canopy not obstructed by leaf or other vegetational material. The LAI index expresses the amount of leaf area per square metre, estimated by a biophysical inversion model (Welles and Norman 1991). CO is directly related to canopy gaps (Canham et al. 1990). LAI is inversely correlated with CO, and both can be correlated with remote sensing images (e.g. Asner et al. 2004).

We used kriging (Cressie 1993) to produce the continuous variables of CO and LAI in both plots. Detailed descriptions of the kriging approach and the semivariogram models used are provided in the online supplemental material (Geostatistical analysis of light environments).

Coarse woody debris of the tree-fall gaps

We estimated the volume of all CWD in each ground gap. CWD was separated into whole dead trees or wood pieces. Whole dead trees (diameter ≥10 cm) were recorded, including snapped bole-falls and uprooted tree-falls. We used the allometric equation developed by Brown (1997) to approximate woody biomass losses by fresh tree-falls and snapped bole-falls. For partial crown-fall we recorded the diameters of all wood pieces ≥10 cm (the end diameter of the logs) and the length of the woody material. We calculated the sectional volume of each segment of CWD using Smalian's equation (1), from the cross-sectional average areas from the ends of the segment:

$$V_s = H(L + U)/2 \tag{1}$$

where V_s is the volume (m^3) of a segment of CWD, H is the segment length (in m), L is the cross-sectional area at the lower end section (large diameter) and U is the cross-sectional area at the upper end section (small end diameter). CWD in the gaps was classified according to its decomposition status (Harmon et al. 1995), into five classes from freshest (class 1) to most rotten (class 5). We used an average of wood density measured for each decay class specifically developed for this site (Keller et al. 2004). The mass of each section of CWD (M_i) was determined from the product of the volume of material (V_i) and the respective density for the material class (ρ_i):

$$M_i = \rho_i V_i \tag{2}$$

We estimated the flux of CWD inside the gap areas by limiting the amount of CWD to recent tree-fall disturbances (< 1-year-old).

Remote sensing data and image processing

Aiming to estimate small disturbances at the scale of tree-fall gaps (Clark et al. 2004a, 2004b) we used high-resolution images from the commercial satellite IKONOS–2. Large disturbances such as blow-downs have been successfully monitored over the Amazon (Nelson et al. 1994; Chambers et al. 2009; Espirito-Santo et al. 2010), but small-scale disturbance remains a challenge. For the latter, two high-resolution images were acquired over the field plots (both off-nadir IKONOS images). The first acquisition was made on June 23, 2008 (ca. two months before the field work campaign) with a nominal collection elevation of 66.77° and sun angle elevation of 56.81°. The second acquisition was conducted on August 11, 2009 (at the same period of field work activities) with a nominal collection elevation of 66.74° and sun angle elevation 54.49°. The IKONOS–2 satellite sensor produces 11-bit radiomeric images in panchromatic and multi-spectral mode with 1 m and 4 m spatial resolution, respectively (Dial et al. 2003). The following image processing steps were applied over the original satellite images: (1) radiometric correction, (2) ortho-rectification, and (3) spectral mixture analysis.

The images were radiometrically transformed from digital numbers to in-band radiance physical units (mW cm^{-2} sr^{-1}). Subsequently the images in radiance units were corrected to the top-atmosphere or apparent reflectance (ρ_a) using the mean solar exo-atmospheric irradiance and the post-calibration gain and off-set (Markham and Barker 1987) of the IKONOS sensor (Taylor 2009), by application of the algorithm developed by Markham and Barker (1987).

We ortho-rectified the IKONOS images using an empirical 3-D rational function model (Toutin 2004) over the rational polynomial coefficients (RPCs) from satellite ephemeris and altitude data (Geo-Eye product). The rational polynomial method is similar to the simple polynomial method, except that it involves a ratio of polynomial transformations. and it also takes ground elevation into consideration. RPCs reduce the numbers of ground control points (GCPs) needed for the ortho-rectification (Toutin 2004). We extracted the Z-terms related to the third dimension of the terrain from an available DEM extracted from the Shuttle Radar Terrain Mission (SRTM) for the region. Although the spatial resolution of SRTM is relatively coarse for high-resolution satellite images (ca. 90 m for South America), this had a minimal effect in our study area since it was flat. In addition we used highly accurate GCPs with differential GPS collected with differential GPS in the field to check the planimetric quality of the ortho-images. A cross-check of GCPs indicated a root mean square (RMS) error of ca. 4 m after the ortho-rectification process (see online supplemental material S1).

We applied a spectral mixture analysis (SMA) by using a linear mixture model (Shimabukuro and Smith 1991) in all four IKONOS multi-spectral bands of both images to produce fractional images based on three end-members: green vegetation (GV), non-photosynthetic vegetation (NPV), and shade (SD). The spectrally pure end-members (GV, NPV and SD) were determined using the pure pixel index (Boardman 1993; Boardman et al. 1995). A spectral library was then built to estimate the fractional proportions (NPV, GV and SD) of each pixel (Shimabukuro and Smith 1991). Bearing in mind the high proportion of shadow in high-resolution images of tropical forest canopy (Asner and Warner 2003) we also produced a simple normalised difference vegetation index (NDVI) (Tucker 1979) from the IKONOS bands in the red (0.632–0.698 μm) and near-infrared (0.757–0.853 μm) for both images.

Linking observed ground disturbance to satellite image

We investigated the relation between ground disturbances and remote sensing data in our 114 ha and 53 ha plots. Considering that ground disturbance is related to the spatial heterogeneity of the light environments (LAI and CO) in the forest canopy, we tested two approaches to link observed ground disturbance to the satellite images. First, we simply tested the direct relationship between light environments collected by hemispherical photographs within each ground gap with its estimated ground gap area collected in the field (Runkle 1981). We then tested the relationship between light environments in the gap areas with the corresponding remote sensing data. Finally, since we did not find any relationship using the earlier approaches, we used the total data collected by LAI–2000 over the two large forest survey plots to investigate the relationship with remote sensing products (unmixing images and NDVI).

We applied an ordinary least-squares regression to assess the relationship between canopy openness (disturbances) and information extracted from high-resolution satellite imagery. The continuous variables of CO and LAI interpolated by kriging (114 and 53 ha plot areas) were used to evaluate the remote sensing IKONOS–2 products, fractions (NPV, GV and SD) and NDVI images. For the 114 ha plots we used a total interpolated grid of 71,416 pixels of 4 m (identical to the spatial resolution of IKONOS–2 multispectral bands) of CO and LAI to evaluate patterns of disturbance in the satellite image of 2008. In the 53 ha plot a total grid of 33,020 pixels of 4 m was used to detect disturbances of tree-fall gaps in the satellite image of 2009. Following the regression analyses we determined the best remote sensing product from IKONOS–2 image (unmixing images and NDVI) to quantify the disturbances at the plot scale and for the whole image. In total we statistically tested 16 variables, of which four were ground remote sensing data (grids of CO and LAI for both plots) and four were satellite products (NPV, GV, SD and NDVI).

We also applied an alternative approach to detect areas with a signal of high ground disturbances. Using the interpolated grids of CO and LAI from both plots, we selected ground thresholds from those variables that were found to cover all mapped polygons of tree-fall gaps. The selected

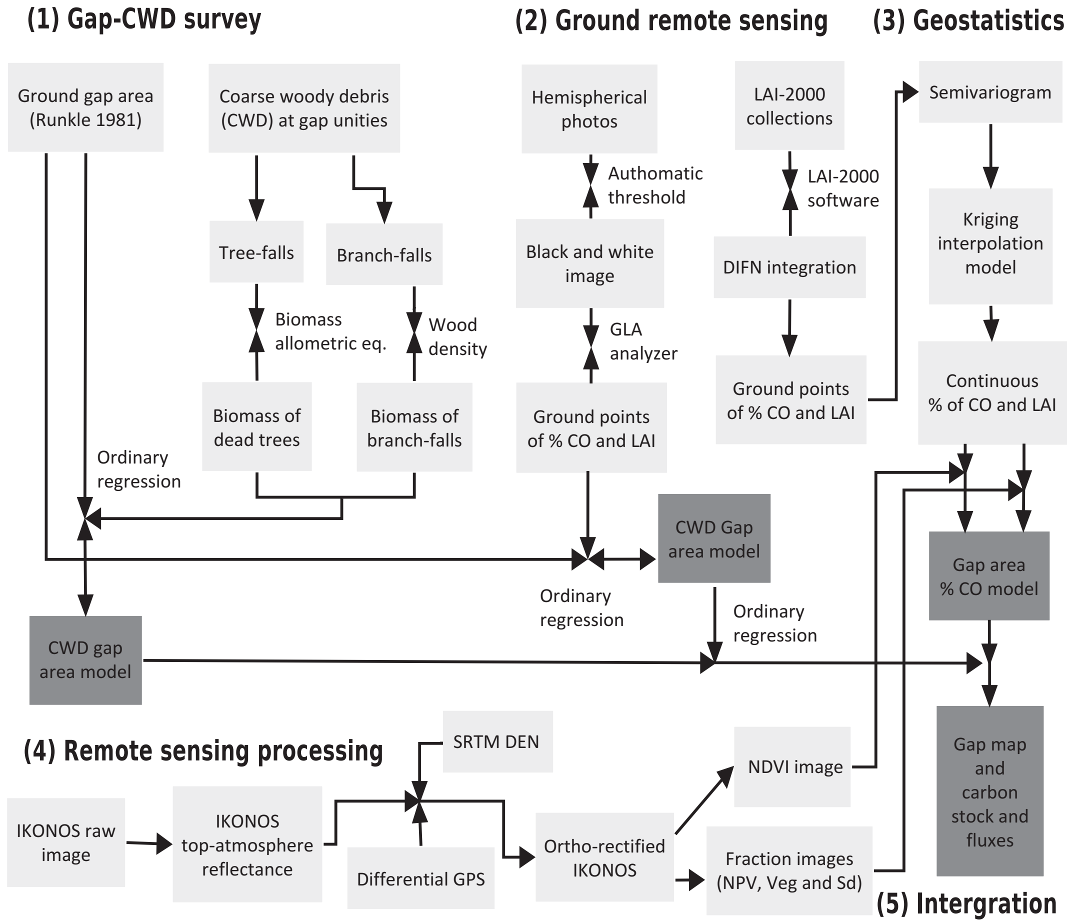

Figure 2. Diagram summarising the methods for the ground gap–CWD survey and remote sensing, geostatistics, image processing and data integration applied in the study.

grid pixels of 4 m from these thresholds were then used in the regression analysis with remote sensing products. We empirically estimated the amount of CWD produced by small-scale disturbances based on this derived remote sensing threshold and on the relation between biophysical canopy gap (CO and LAI) and CWD. Our methodological approach is summarised in Figure 2.

Results

Gap geometry, CWD and tree mortality

In the two large forest inventory plots totalling 167 ha (114 and 53 ha) we found 96 gaps. We removed four samples (outliers), reducing our total sample to $n = 92$ (Table 1). Outliers were identified by plotting the residuals in stepwise scatter plot pairs with high scores of leverage (the impact on the fitted values when i-*th* cases are dropped from the regression models) (Crawley 2007). These four outliers had a large amount of CWD and numbers of dead trees for a small proportion of opened area. The correlation between CWD and gap area increased from $r = 0.61$ to $r = 0.73$ after exclusion of the outliers. In addition, after removing the outliers the correlation between the number of dead trees and the gap area increased from $r = 0.69$ to $r = 0.75$.

We found a total of 16 gaps produced by partial or complete crown-fall (either from live or dead standing trees), 44 by snapped bole-fall and 32 by uprooted tree-fall (Table 1). In total these disturbances represented an area of 2.37 ha, or 1.42% of the whole area surveyed. Only 1.36 ha, or 0.81%, of the plots was affected by recent disturbances (<1-year-old). The recurrence interval or turnover for these events was calculated as about 123 years for all gap formation types. The mean gap size was 257 m^2 (95% confidence limit between 219 and 294 m^2). The minimum gap size was 32 m^2 (crown-fall) and the maximum 1,313 m^2 (uprooted tree-fall). The average length of these gaps was 26 m where the geometry of uprooted gaps had the largest length (81 m), and consequently the largest disturbance area.

Amounts of CWD depended on the type of gap formation, crown-falls contained 0.11 Mg C ha^{-1} of CWD, snapped tree-falls 0.65 Mg C ha^{-1} and uprooted tree-falls 0.70 Mg C ha^{-1}. In total, the 92 gaps contained a stock of 1.45 Mg C ha^{-1} of necromass for the study area. The flux of CWD caused by the gaps was 0.76 Mg C ha^{-1} $year^{-1}$. The average mortality of trees (DBH $\geq$10 cm) per gap was 6.5, resulting in a total of 596 dead individual trees (3.57 trees ha^{-1} >10 cm DBH) for the total surveyed area of 167 ha. From the total dead trees of all ages contained in the gaps,

Table 1. Mode of gap formation and disturbance responses (number of dead trees, above-ground biomass and coarse woody debris (CWD) in two plots of 114 ha and 53 ha forest surveys in the Tapajós National Forest, Pará State, Brazil.

	Mode of gap formation			
Gap parameters	Crown-fall	Snapped	Uprooted	All gap types
Frequency of gap formation mode	16	44	32	92
Proportion of gap formation mode (%)[a]	17	48	35	100
Gap area (ha)	0.26	1.18	0.93	2.37
Proportion of plot area under gap (%)[b]	0.15	0.71	0.56	1.42
Gap area (ha) with <1-year-old in 167 ha	0.14	0.90	0.32	1.36
Proportion of plot area under gaps <1-year-old (%)	0.08	0.54	0.19	0.81
Frequency of gaps >500 m^2	0	4	2	6
Maximum gap size (m^2)	266	658	1313	1313
Minimum gap size (m^2)	32	92	100	32
Mean gap size (m^2)	160	268	290	257
Median gap size (m^2)	187	232	251	220
Standard deviation gap size (m^2)	67	146	242	182
Maximum gap perimeter (m)	72	123	192	192
Minimum gap perimeter (m)	22	37	40	22
Mean gap perimeter (m)	50	69	74	67
Median gap perimeter (m)	54	62	70	65
Standard deviation of gap perimeter (m)	14	22	32	26
Maximum gap length (m)	32	49	82	82
Minimum gap length (m)	7	13	15	7
Mean gap length (m)	19	25	31	26
Median gap length (m)	19	24	27	24
Standard deviation of gap length (m)	6	9	15	12
Maximum gap width (m)	18	29	33	33
Minimum gap width (m)	4	7	6	4
Mean gap width (m)	12	14	13	13
Median gap width (m)	13	14	13	13
Standard deviation of gap width (m)	3.92	4.37	5.62	4.80
Maximum CWD per gap (Mg C)[c]	2.85	8.79	17.55	17.55
Minimum CWD per gap (Mg C)[c]	0.06	0.14	0.40	0.06
Mean CWD per gap (Mg C)[c]	1.12	2.45	3.63	2.63
Median CWD per gap (Mg C)[c]	1.18	1.46	2.94	1.61
Standard deviation of CWD per gap (Mg C)[c]	0.74	2.23	3.47	2.7
CWD in gaps (Mg C ha^{-1})[c]	0.11	0.65	0.70	1.45
CWD flux in gaps (Mg C ha^{-1} $year^{-1}$)[d]	0.05	0.45	0.26	0.76
Maximum number of dead trees per gap[e]	10	24	26	26
Minimum number of dead trees per gap[e]	0	1	1	0
Mean number of dead trees per gap[e]	2.7	7.8	6.6	6.5
Median number of dead trees per gap[e]	1.5	6.5	5	5
Standard deviation of dead trees per gap[e]	2.65	5.87	6.03	5.77
Dead trees in the gaps per hectare[e]	0.25	2.05	1.27	3.57
Annual tree mortality per hectare[f]	0.19	1.68	0.51	2.38

[a]Proportion = (sum area of gaps in all ages/total gap area) × 100%.
[b]Proportion = (sum area of gaps <1-year-old/total plot area) × 100%.
[c]Only pieces of CWD ≥10 cm of diameter were measured in gaps of all ages.
[d]Only pieces of CWD ≥10 cm of diameter were measured in gaps <1-year-old.
[e]Only dead trees ≥10 cm of diameter at breast height were measured in the gaps of all ages.
[f]Only dead trees ≥10 cm of diameter at breast height were measured in the gaps <1-year-old.

we estimated a mean annual tree mortality of 2.38 trees ha^{-1} $year^{-1}$ (Table 1).

Linking gap geometry and light penetration to carbon stocks

There was a strong correlation between production of CWD and gap geometry ($r = 0.73$ for area, $r = 0.80$ for perimeter and $r = 0.78$ for length) (Figure 3 and online supplemental material, S19). Gap area and perimeter were both correlated ($r = 0.75$ and 0.77, respectively) with the number of dead trees (Figure 3 and online supplemental material, S20).

We found a weak correlation between CWD and ground hemispherical photo measurements of CO and LAI ($r = 0.22$ and $r = 0.12$, respectively). A higher correlation was found between the number of dead trees and these variables ($r = 0.57$ for CO and $r = 0.41$ for LAI). A total of 184 hemispherical photos were collected (two for each gap) and analysed with GLA (Frazer et al. 1999) to estimate CO ($n = 92$) and LAI ($n = 92$) for each gap.

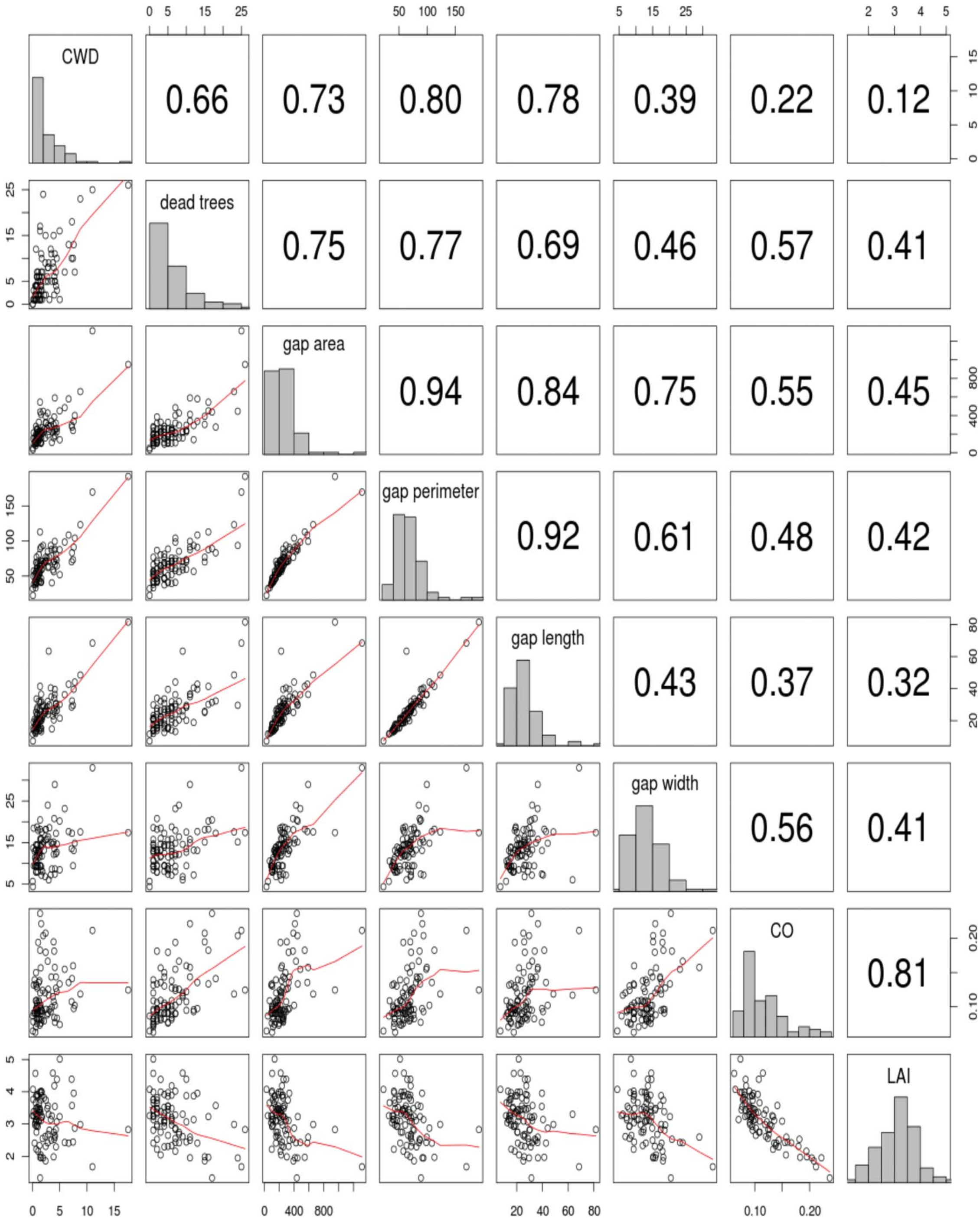

Figure 3. Bivariate Pearson correlation coefficients (r) between pairs of gap parameters (displayed on the diagonal) of the gap survey ($n = 92$) in two large forest plots (114 and 53 ha) in the Tapajós National Forest, Pará State, Brazil. CWD in Mg C; number of dead trees >10 cm of DBH; gap area in m^2; gap length and width in m; CO, proportion of canopy openness; LAI, leaf area index. Values above the diagonal are linear correlation coefficients; below the diagonal scatter plots of variable pairs are shown, fit with a non-linear parametric smoothing function (Crawley 2007).

Remote sensing and forest light environments

Based on the high-resolution multispectral bands of the IKONOS–2 acquired close to the dates of our forest surveys, we produced the remote sensing products NDVI and spectral unmixing fraction images (GV, NPV and SD) for the 114 ha (Figure 4) and 53 ha (online supplemental material, S2) plots.

Geostatistical analysis of CO and LAI in the 114 ha plot ($n = 731$) indicated a spatial auto-correlation of both variables (online supplemental material, S13) to a range of 56 and 71 m for CO and LAI, respectively (online supplemental material, S2(a)–(b)). For the 53 ha plot ($n = 2315$) a stronger pattern of spatial auto-correlation was found to a range of 57 and 60 m for CO and LAI, respectively (online

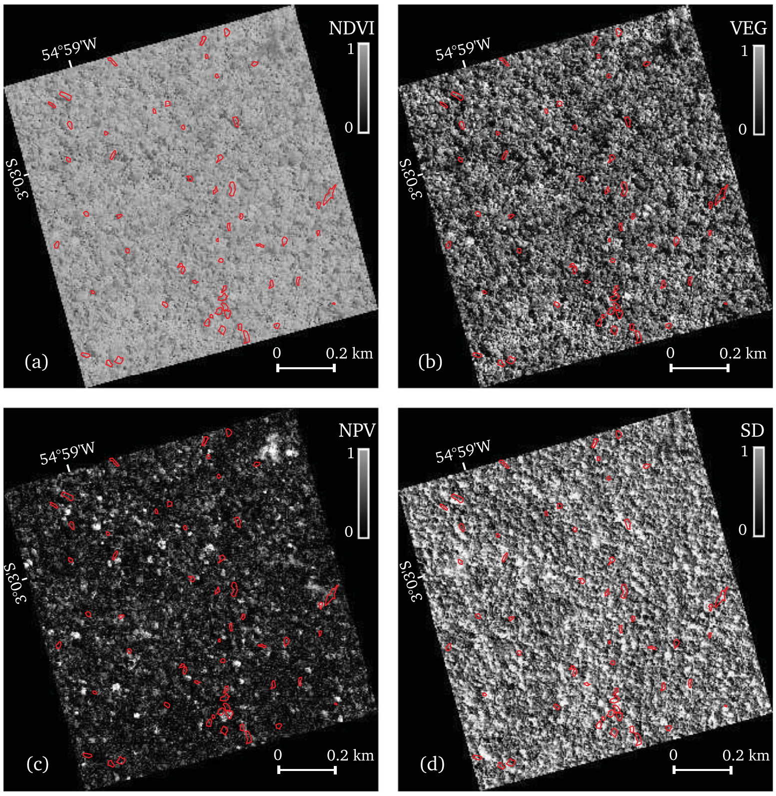

Figure 4. IKONOS-2 image processing of the 114 ha plot in the Tapajós National Forest, Pará State, Brazil: (a) normalised difference vegetation index (NDVI), (b) unmixing fraction images of green vegetation GV, (c) non-photosynthetic vegetation NPV, and (d) shade SD. Ground gaps ($n = 55$) are overlaid in red.

supplemental material, S2(c)–(d)). We found a spatial trend in both CO and LAI for the data of the 114 ha plot, probably related to the dissected relief, but no spatial trend in CO and LAI for the 53 ha plot (online supplemental material, S5–10). Semivariograms of the data for both large plots showed a periodic variance every 50 m (online supplemental material, S11–12), aliasing the spacing between transects. Based on the smallest RMSE for both types of data we selected and fitted an isotropic exponential semivariogram model:

$$\gamma(h) = c_0\,[1 - \exp(-h/a_0)], \tag{3}$$

where $\gamma(h)$ is the semivariance at the lag h, c_0 is the variance asymptote and a_0 the lag distance or range.

A clear pattern of light penetration was found around the ground gaps of the 114 ha plot (Figure 5(a) and (f)) and the 53 ha plot (online supplemental material, S18(a) and (f)), although the uncertainty of interpolation was high for the 114 ha plot due to the lower density of data collected (online supplemental material, S15 and S16). The geostatistical interpolation of canopy openness (the square root of CO) and LAI clearly showed that the occurrence of gaps increased the light penetration at the forest floor in both plots (Figure 5(a) and online supplemental material, S18(a)). Tree-fall gaps increased the amount of open sky and reduced the total LAI (Figure 5(f) and online supplemental material, S18(f)). We found that most gaps occurred in areas with CO $\geq$0.25 and LAI $\leq$4 indices in both plots.

We were unable to find any significant correlation between remote sensing spectral products (NDVI and GV, NPV and SD unmixing images) and the continuous biophysical variables – interpolated values of CO (Figure 5(b)–(e)) and LAI (Figure 5(g)–(j)) of the 114 ha plot (total grid with $n = 71{,}416$ pixels of 4 m), or in the 53 ha plot (online supplemental material, S18, total grid with $n = 33{,}020$ pixels of 4 m). Similarly, we were unable to find any significant correlation between the remote sensing products and raw ground data points (CO and LAI) in the 114 ha ($n = 731$) or 53 ha ($n = 2315$) plots (data not shown).

As gaps produced a large variability of light environments, thresholds of CO and LAI were selected in both large grids to identify ground disturbances inside the satellite images. For the 114 ha plot the comparison between areas where CO values were $\geq$0.30 and LAI $\leq$4 and remote sensing products showed no correlation (online supplemental material, S16). For the 53 ha plot the regression analysis between areas where CO $\geq$0.23 and LAI $\leq$5 and remote sensing products also showed also no correlation (online supplemental material, S17).

The overlay of the canopy gaps of the 114 ha plot recorded in the field over the 1 m spatial resolution panchromatic IKONOS–2 image (Figures 6(a) and 6(c)) and its 4 m multispectral unmixing images of VG, NPV and SD

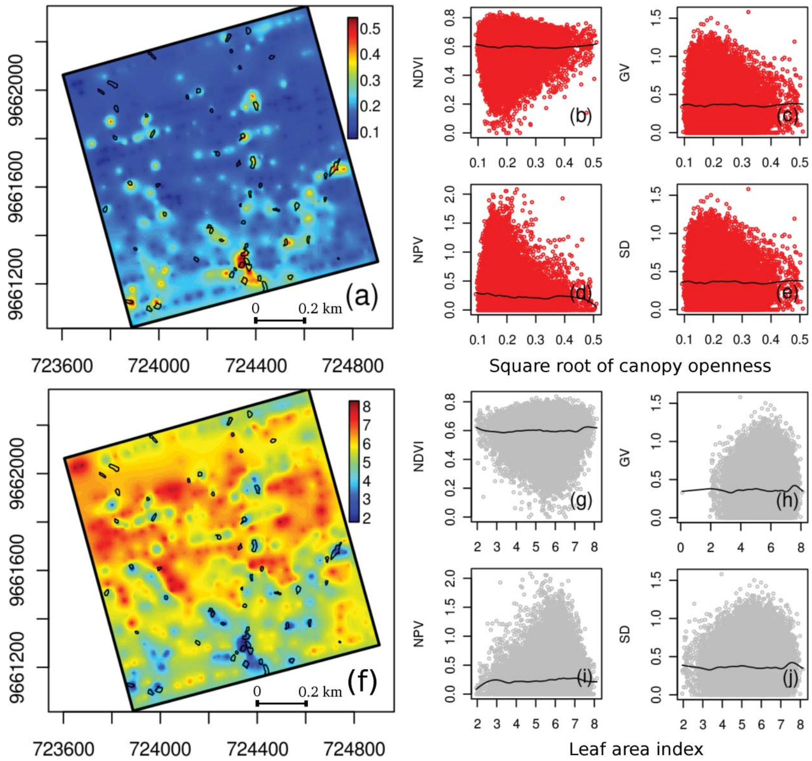

Figure 5. Interpolated ground collections ($n = 731$) of canopy openness (square root values, (a)) and leaf area index (LAI, f) in a 114-ha forest plot (4-m grid plot), using kriging with an exponential semivariogram model, in the Tapajós National Forest, Pará State, Brazil. Gaps, shown as black polygons in (a) and (f) are present in areas of high CO (a), and low LAI (f). Scatter plots of canopy openness grid and remote sensing products (4 m spatial resolution): NDVI (b) green vegetation (c), non-photosynthetic vegetation (NPV, d) and shade (SD). For the LAI grid plot the scatter plots with the same remote sensing products are: NDVI (g), green vegetation (h), non-photosynthetic vegetation (i) and shade (j).

(Figures 6(b) and 6(d)) indicated that most of the ground gaps were located in areas with a high SD in the image (Figure 6(d)). We found an identical pattern of high proportion of shadow component in areas of tree-fall gaps over the second high-resolution image of the 53 ha plot (Figure not shown).

Discussion

In the Tapajós National Forest the major mode of gap formation was snapped bole tree-fall (Table 1, $n = 44$ from a total of 92 gaps), suggesting that tall trees of the forest canopy were killed by winds associated with the rainy season (Garstang et al. 1998) or the low-level winds driven by the mesoscale circulations of the Amazon and Tapajós rivers (Lu et al. 2005). Several large trees (DBH $\geq$50 cm) had trunks broken at a height around 5 to 8 m, which suggests strong patterns of wind gusts at the forest canopy.

In our study we found a strong relationship between tree mortality and gap size (Figure 3). Of the 92 gaps, only 16 disturbances resulted from a single tree-fall. Many individual tree deaths resulted in no quantified gap formation, using Runkle's gap definition. Most gaps resulted from multiple fallen trees, with an average mortality of 6.5 trees (>10 cm DBH) per gap (Table 1). As expected, more fallen trees produced larger gaps, and we found a high correlation between the number of dead trees and gap area ($r = 0.75$) or gap perimeter ($r = 0.77$) (Figure 3 and online supplemental material, S20), a relationship that has not previously been quantified in tropical forests.

We are also able to provide the first statistics in the tropical forest literature of CWD production based on gap size and mode of gap formation (Figure 3 and online supplemental material, S19). Gap formation as a result of uprooted tree-falls produced one and a half times more CWD per gap than snapped boles, and three times more than crown-falls, probably because uprooted trees have a higher wood density and biomass than those created through other modes of tree mortality (Chao et al. 2009). Uprooted tree-falls created larger gaps areas (average ca. 290 m^2) than others types of gap formation.

Estimates of carbon fluxes based on tree mortality from permanent plot studies differ from those derived from gap formation rates (Leigh 1975). For example, a snapped-off tree may not die, even when much biomass is lost. Conversely, a tree that dies standing may never form a gap. We compared our results with permanent forest plots (Pyle et al. 2008) for tree mortality measurements and repetitive line intercept transects for monitoring of CWD flux (Palace et al. 2008) in the TNF. In our study plots, gap disturbances accounted for a mean tree mortality of 2.4 stems ha^{-1} year^{-1} (>10 cm of DBH), while Pyle et al. (2008) found rates of 8.4 stems ha^{-1} year^{-1} (>10 cm of DBH). The total stock of CWD in gaps represented between 4.9% and 5.8%

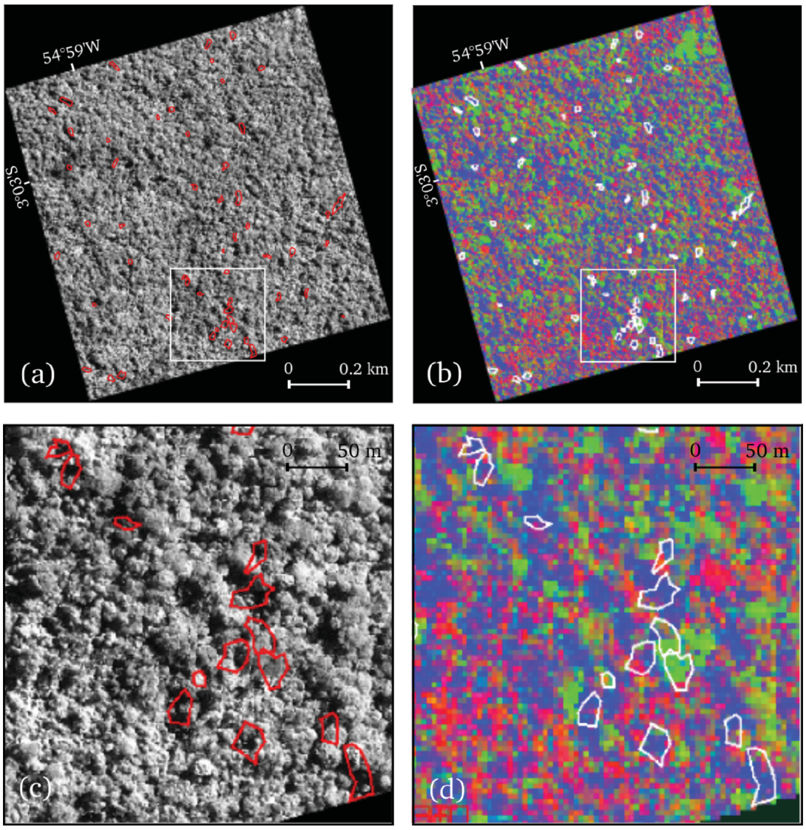

Figure 6. Distribution of ground gaps (red lines, $n = 55$) over 1 m spatial resolution panchromatic IKONOS-2 image of 23 June 2008 with full-width wavelength 0.45–0.90 μm (a) and RGB colour composition of the unmixing images of green vegetation, non-photosynthetic vegetation and shade (b), respectively, in the Tapajós National Forest, Pará State, Brazil; spatial details of ground gaps in the panchromatic high-resolution image (c), and spectral details of the gaps in the unmixing images (d).

of the total stock of the fallen CWD, when compared with Palace et al. (2008) and Pyle et al. (2008), respectively. The production of CWD in recent gaps (<1-year-old) was 0.76 Mg C ha^{-1} year^{-1}. This represented only 29% the size of the flux of carbon from annual tree mortality measured by Pyle et al. (2008), or 23% of the total new flux of CWD (Palace et al. 2008).

In a study in Panama, Young and Hubbel (1991) showed that gaps were persistent. Our data, showing relatively low necromass density in gaps, are consistent with this interpretation. The recurrence interval or turnover for gap area formation in our study was about 123 years, falling within the average range of 100–125 years in other studies (Denslow 1987; Brokaw 1982; van der Meer et al. 1994), although these studies used different gap definitions. If we had calculated the recurrence interval for our study based on the carbon flux of CWD inside the gaps, then the time would have been noticeably longer (197 years). By comparison, the calculated carbon turnover based on tree mortality (ca. 3 Mg C ha^{-1} year^{-1}) and stock of above-ground biomass (150 Mg C ha^{-1}) (Pyle et al. 2008) at TNF is 50 years. The median turnover time calculated by Malhi et al. (2004) for nearly 100 neotropical forest plots was approximately 50 years. The very long turnover time for carbon cycling by gaps at the TNF indicates that gap-forming mortality accounts for only a portion of woody carbon turnover.

While a great deal of research on canopy disturbance regimes and the response of individual species to gaps has been documented, there has been remarkably little research on the spatial pattern of forest light regimes in and around gaps (Canham et al. 1990) for larger areas. In our study, despite the differences of sample design between plots (50 m × 15 m vs. 25 m × 15 m) and the quantity of data collected ($n = 731$ vs. $n = 2315$), the geostatistical interpolation of canopy openness (the square root of CO) and LAI indicate that the occurrence of tree-fall gaps increased CO (Figure 5(a) and online supplemental material, S18(a)) and reduced the total of LAI (Figure 5(f) and online supplemental material, S18(f)) at values of CO $\geq$0.23 and LAI $\leq$4 in gap areas (online supplemental material, S16 and S17). It is interesting to note that the spatial autocorrelation of light measurements had a range of about 56 to 71 m (online supplemental material, S13), comparable to the height of the tallest trees in this forest (Lefsky et al. 2005). It is also possible that the 25 m and 50 m spacing of the sample lines may have been aliased into the spatial signal.

Light penetration is affected beyond the gap, and the ecologically altered area at the forest floor is often larger than the size of the gap at the forest canopy level (Popma et al. 1988). Runkle's gap definition is normally assumed to be a reasonable measure of the gap size at the forest floor, and Brokaw's gap size is taken in the forest canopy (Clark 1990). Gaps measured according to the Brokaw definition are between two and three times smaller than Runkle's gap area (van der Meer et al. 1994). Over the 167 ha area of our study plots, 1.42% of this plot was defined as gap according to the Runkle definition (Table 1). Using an empirical threshold of light penetration of CO $\geq$0.30 (114 ha plot) and CO $\geq$0.23 (53 ha plot) where most of the gaps were geographically located (online supplemental material, 16(a) and 17(a)), the gaps accounted for 2.57% and 3.33% of the total area of the 114 ha and 53 ha plots, respectively. Comparing our instrumental measurement of light penetration with gaps measured on the ground (Runkle 1981), we found that the area measured by LAI–2000 PCA was twice as large as the areas defined by Runkle, or a factor of as much as 4 using the conservative gap definition of Brokaw (1982).

These last results are in accordance with the earlier opinion of Lieberman and Lieberman (1989) that the dichotomous definition of forest environments into gap and non-gap is unrealistic. Further quantitative studies of the spatial distribution of light environments at the forest floor (continuous data) are needed to understand the effects of natural disturbance at the canopy forest structure (e.g. LAI) and function (e.g. photosynthesis).

Passive optical remote sensing data have been used previously to estimate areas for large tropical forest disturbances (Nelson et al. 1994; Chambers et al. 2007, 2009; Espírito-Santo et al. 2010), and this technique has also been employed to quantify the areas and damage caused by logging (e.g. Read et al. 2003; Asner et al. 2004). To a limited extent, high-resolution optical remote sensing has been used to identify mortality in emergent canopy trees (Clark et al. 2004b). We tested whether high spatial resolution satellite images (IKONOS–2) could be used to estimate gap formation in unmanaged old growth forest. We found no correlation between the derived variables (NDVI, GV, NPV and SD) from remote sensing images and CO or LAI, using data from the entire plots or for a sub-set of the data in gaps (online supplemental material, S16 and S17). Inspection of the images suggested that for the present example of Amazonian forest, ground measurements of CO and LAI and remote sensing products (16 covariates) failed to show significant correlation, due to the effect of shadows (Figure 6). The shadow fraction represents ca. 30% ($\pm$10% SD) of the area in high-resolution images of old growth tropical forests and thus exerts a major influence on spatial variability in canopy reflectance, at both local and regional levels (Asner and Warner 2003). Gaps are by definition associated with a high proportion of shadow (Figure 6). However, due to the variable canopy height in old-growth forest, shadows are also abundant in non-gap areas of the heterogeneous forest canopy. It was therefore not possible to specifically detect gaps using automated spectral methods by means of the high-resolution IKONOS–2 images.

Commercial high-resolution acquisition of remotely sensed images tends to be significantly off-nadir (Toutin 2004; Taylor 2009). A requirement for near-nadir acquisition in the tropics would be constrained because of cloud cover or mission priority resulting in high acquisition costs. Even at relatively favourable nominal collection elevation (>70°), prior results indicate that interpretation would be sensitive to the shadow fraction. Asner and Warner (2003) calculated that a 10% increase in shadow fraction at red wavelengths (0.63–0.69 μm) resulted in a 3% decrease in pixel reflectance. Multiple images at different view geometries might be used to address the shadow problem, but this approach would still be limited by cloudiness. It would also increase costs linearly with the number of images, and would add a new problem of temporal de-correlation – the forest changes dynamically and it would be very difficult to acquire multiple images at the same time, and it would also be difficult to minimise the sensitivity to shadows in a study with limited resources. Use of the current generation of commercial optical satellite sensors that might be able to overcome the shadow problems (satellite images with nominal collection >70°) would be very costly.

Due to the complex structure of the old-growth forest, shade areas are not uniquely associated with gaps. Emergent trees produce shade, even where there is no canopy gap. Based on the published literature (Asner and Warner 2003) we had expected that a high fraction of shadow would be present, but we expected that image normalisation (e.g. NDVI filtering) or de-convolution into components (e.g. mixture modelling) might resolve the shadow problem. However, we found out that the shadows were resistant to these treatments.

It is noted that IKONOS–1 images have been used in the TNF to map recent man-made canopy gaps caused by selective logging activities, by application of NDVI thresholds and visual interpretation (Miller et al. 2007). Despite the recognition that NDVI is an effective index for reducing the effect of remote sensing artefacts from solar geometry effects, acquisition image angles, noise and atmosphere contaminations, shadow and topography (Tucker 1979), we found that NDVI filtering alone was insufficient to permit gap detection. Textural cues (tracks of logging roads and skid trails) were probably critical to the visual interpretation of logging gap areas by Miller et al. (2007).

In future studies it is intended that the spectral approach to image interpretation may be replaced or supplemented or by other techniques to extract information on gaps from the high-resolution images. The modern currently available techniques of image processing or computer vision using textural metrics (Kayitakire et al. 2006; Malhi and Román-Cuesta 2008) could be very useful for detecting patterns of disturbances in high-resolution satellite images.

In conclusion, it must be emphasised that for the first time we have been able to quantify the relationship between gap area and tree mortality, and gap area and CWD production. These strong relationships will be useful for quantifying carbon fluxes from gap creation by the use of remote sensing, provided a suitable remote sensing approach can be found for quantifying gap area. The correlation between gap area disturbance intensity may be useful for extrapolating disturbance areas detected by remote sensing to carbon cycling on the regional scale (Chambers et al.

2007). However, we wish to point out that in the case of old-growth forest that we have studied, fewer than 30% of mortality events resulting in gap formation as measured on the ground. Remote sensing studies of gap formation alone are therefore not sufficient for quantifying tree mortality in old-growth tropical forests.

Acknowledgements

We are grateful to the Journal editors David Galbraith and Laszlo Nagy and three anonymous referees for their constructive comments on earlier versions of the manuscript.

This research was supported by the NASA Earth System Science Fellowship (NESSF) (Grant # NNX07AN84N) and the NASA Terrestrial Ecology Program contribution to the Large Scale Biosphere–Atmosphere Experiment in the Amazon (LBA).

We thank the Brazilian Ministry of Science and Technology for its support of the LBA programme and the National Institute for Amazon Research for the implementation of this programme.

Notes on contributors

Fernando D.B. Espírito-Santo is a CalTech Postdoctoral Scholar. He has a Ph.D. from the University of New Hampshire and has worked extensively in the Brazilian Amazon forests since 2001.

Michael Keller was NASA project scientist for the LBA–ECO component of the Brazilian-led LBA. He is an affiliate professor at the University of New Hampshire and a Research Scientist at the International Institute of Tropical Forestry, US Forest Service.

Ernst Linder is a professor who has worked with spatial and temporal statistics of a number of environmental studies.

Raimundo Cosme Oliveira Junior is a researcher who has worked on agriculture and forestry in the Amazon.

Cleuton Pereira has worked on forest inventories in the Amazon.

Cleber G. Oliveira has a Ph.D. from the National Institute Space Research (INPE) in Brazil and has worked on Amazon geology.

References

Asner GP, Keller M, Pereira JR, Zweede, JC, Silva JN. 2004. Canopy damage and recovery following selective logging in an Amazon forest: Integrating field and satellite studies. Ecological Applications 14:S280–S298.

Asner GP, Palace M, Keller M, Pereira Jr R, Silva JNM, Zweede JC. 2002. Estimation of canopy structure in an Amazon forest from laser range finder and IKONOS satellite observations. Biotropica 34:483–492.

Asner GP, Warner AS. 2003. Canopy shadow in IKONOS satellite observations of tropical forests and savannas. Remote Sensing of the Environment 83:521–533.

Baker TR, Phillips OL, Malhi Y, Almeida S, Arroyo L, Di Fiore A, Erwin T, Killeen TJ, Laurance SG, Laurance WF, et al. 2004. Variation in wood density determines spatial patterns in Amazonian forest biomass. Global Change Biology 10:545–562.

Barbier N, Couteron P, Proisy C, Malhi Y, Gastellu-Etchegorry JP. 2010. The variation of apparent crown size and canopy heterogeneity across lowland Amazonian forests. Global Ecology and Biogeography 19:72–84.

Boardman JW. 1993. Automating spectral unmixing of AVIRIS data using convex geometry concepts. In: Summaries of the Fourth Annual JPL Airborne Geoscience Workshop. Pasadena (CA): JPL.

Boardman JW, Kruse FA, Green RO. 1995. Mapping target signatures via partial unmixing of AVIRIS data. In: Summaries of the Fifth Annual JPL Airborne Geoscience Workshop. Pasadena (CA): JPL.

Brokaw NVL. 1982. The definition of treefall gap and its effect on measures of forest dynamics. Biotropica 14:158–160.

Brokaw NVL, Scheiner SM. 1989. Species composition in gaps and structure of a tropical forest. Ecology 70:538–541.

Brown S. 1997. Estimating biomass and biomass change of tropical forests: a primer. Rome (Italy): FAO Forest Paper 134.

Canham CD, Denslow JS, Platt WJ, Runkle JR, Spies TA, White PS. 1990. Light regimes beneath closed canopies and tree-fall gaps in temperate and tropical forests. Canadian Journal of Forest Research-revue Canadienne De Recherche Forestiere 20:620–631.

Chambers JQ, Higuchi N, Teixeira LM, Santos J, Laurance SG, Trumbore SE. 2004. Response of tree biomass and wood litter to disturbance in a Central Amazon forest. Oecologia 141:596–611.

Chambers JQ, Fisher JI, Zeng H, Chapman EL, Baker DB, Hurtt GC. 2007. Hurricane Katrina's carbon footprint on US Gulf Coast forests. Science 318:1107–1108.

Chambers JQ, Robertson A, Carneiro V, Lima A, Smith M-L, Plourde L, Higuchi N. 2009. Hyperspectral remote detection of niche partitioning among canopy trees driven by blowdown gap disturbances in the Central Amazon. Oecologia 160:107–117.

Chao KJ, Phillips OL, Monteagudo A, Torres-Lezama A, Martinez RV. 2009. How do trees die? Mode of death in northern Amazonia. Journal of Vegetation Science 20:260–268.

Clark DB. 1990. The reproductive biology of tropical plants. In: KS Bawa, M Hadley, editors. Man and the biosphere series. London: The Parthenon. p. 291–315.

Clark DB, Castro CS, Alvarado LDA, Read JM. 2004a. Quantifying mortality of tropical rain forest trees using high-spatial-resolution satellite data. Ecology Letters 7:52–59.

Clark DB, Clark DA. 2000. Landscape-scale variation in forest structure and biomass in a tropical rain forest. Forest Ecology and Management 137:185–198.

Clark DB, Clark DA, Brown S, Oberbauer SF, Veldkamp E. 2002. Stocks and flows of coarse woody debris across a tropical rain forest nutrient and topography gradient. Forest Ecology and Management 164:237–248.

Clark DB, Read JM, Clark ML, Cruz AM, Dotti MF, Clark DA. 2004b. Application of 1-m and 4-m resolution satellite data to ecological studies of tropical rain forests. Ecological Applications 14:61–74.

Crawley MJ. 2007. The R book. Hoboken, NJ: John Wiley & Sons.

Cressie N. 1993. Statistics for spatial data. Revised Edition. Hoboken, NJ: Wiley–Interscience.

Delaney M, Brown S, Lugo AE, Torres-Lezama A, Quintero NB. 1997. The distribution of organic carbon in major components of forests located in five life zones of Venezuela. Journal of Tropical Ecology 13:697–708.

Denslow JS. 1987. Tropical rainforest gaps and tree species diversity. Annual Review of Ecology and Systematics 18:431–451.

Dial G, Bowen H, Gerlach F, Grodecki J, Oleszczuk R. 2003. IKONOS satellite, imagery, and products. Remote Sensing of the Environment 88:23–36.

Espírito-Santo FDB, Keller M, Braswell B, Nelson BW, Frolking S, Vicente G. 2010. Storm intensity and old-growth forest disturbances in the Amazon region. Geophysical Research Letters 37:L11403.

Fields T. 2006. Tools for spatial data. National Center for Atmospheric Research.

Frazer GW, Canham CD, Lertzman KP. 1999. Gap light analyzer: Imaging software to extract canopy structure and gap light transmission indices from true-colour fisheye photographs, users manual and program documentation. Burnaby (BC) and the Institute of Ecosystem Studies, Millbrook (NY): Simon Fraser University.

Frazer GW, Fournier RA, Trofymow JA, Hall RJ. 2001. A comparison of digital and film fisheye photography for analysis of forest canopy structure and gap light transmission. Agricultural and Forest Meteorology 109:249–263.

Garstang M, White S, Shugart HH, Halverson J. 1998. Convective cloud downdrafts as the cause of large blowdowns in the Amazon rainforest. Meteorology and Atmospheric Physics 67:199–212.

Harmon ME, Whigham DF, Sexton J, Olmsted I. 1995. Decomposition and mass of woody detritus in the dry tropical forests of the northeastern Yucatan Peninsula, Mexico. Biotropica 27:305–316.

Hubbell SP, Foster RB, O'Brien ST, Harms KE, Condit R, Wechsler B, Wright SJ, Loo de Lao S. 1999. Light-gap disturbances, recruitment limitation, and tree diversity in a neotropical forest. Science 283:554–557.

Kayitakire F, Hamel C, Defourny P. 2006. Retrieving forest structure variables based on image texture analysis and IKONOS–2 imagery. Remote Sensing of the Environment 102:390–401.

Keller M, Palace M, Asner G, Pereira R, Silva JN. 2004. Coarse woody debris in undisturbed and logged forests in the eastern Brazilian Amazon. Global Change Biology 10:784–795.

Keller M, Palace M, Hurtt G.E. 2001. Biomass in the Tapajos National Forest, Brazil: Examination of sampling and allometric uncertainties. Forest Ecology and Management 154:371–382.

Lefsky MA, Harding DJ, Keller M, Cohen WB, Carabajal CC, Espírito-Santo FDB, Hunter MO, Oliveira R, Camargo PB. 2005. Estimates of forest canopy height and aboveground biomass using ICESat. Geophysical Research Letters 32:L22S02.

Leigh EG. 1975. Structure and climate in tropical rain forests. Annual Review of Ecology and Systematic 6:67–86.

Li–COR. LAI–2000 plant canopy analyzer: operation manual. Lincoln, NE.

Lieberman M, Lieberman D. 1989. Forests are not just Swiss cheese: canopy stereogeometry of non-gaps in tropical forests. Ecology 70:550–552.

Lu LX, Denning AS, da Silva-Dias MA, da Silva-Dias P, Longo M, Freitas SR, Saatchi S. 2005. Mesoscale circulations and atmospheric CO_2 variations in the Tapajós Region, Pará, Brazil. Journal of Geophysical Research-Atmospheres 110:D21102.

Malhi Y, Baker TR, Phillips OL, Almeida S, Alvarez E, Arroyo L, Chave J, Czimczik CI, Di Fiore A, Higuchi N, et al. 2004. The above-ground coarse wood productivity of 104 neotropical forest plots. Global Change Biology 10:563–591.

Malhi Y, Román-Cuesta RM. 2008. Analysis of lacunarity and scales of spatial homogeneity in IKONOS images of Amazonian tropical forest canopies. Remote Sensing of Environment 112:2074–2087.

Markham BL, Barker JL. 1987. Radiometric properties of U.S. processed Landsat MSS data. Remote Sensing of the Environment 22:39–71.

Miller SD, Goulden ML, Da Rocha HR. 2007. The effect of canopy gaps on subcanopy ventilation and scalar fluxes in a tropical forest. Agricultural and Forest Meteorology 142:25–34.

Nelson BW, Kapos V, Adams JB, Oliveira WJ, Braun OPG, Amaral IL. 1994. Forest disturbance by large blowdowns in the Brazilian Amazon. Ecology 75:853–858.

NOAA. 2010. Estimated value of magnetic declination. Washington (DC): NOAA.

Nobis M, Hunziker U. 2005. Automatic thresholding for hemispherical canopy-photographs based on edge detection. Agricultural and Forest Meteorology 128:243–250.

Palace M, Keller M, Asner GP, Silva JNM, Passos C. 2007. Necromass in undisturbed and logged forests in the Brazilian Amazon. Forest Ecology Management 238:309–318.

Palace M, Keller M, Silva H. 2008. Necromass production: Studies in undisturbed and logged Amazon forests. Ecological Applications 18:873–884.

Phillips OL, Malhi Y, Higuchi N, Laurance WF, Núnez PV, Vásquez RM, Laurance SG, Ferreira LV, Stern M, Brown S, Grace J. 1998. Changes in the carbon balance of tropical forests: evidence from long-term plots. Science 282:439–442.

Popma J, Bongers F, Martinezramos M, Veneklaas E. 1988. Pioneer species distribution in treefall gaps in neotropical rain-forest – a gap definition and its consequences. Journal of Tropical Ecology 4:77–88.

Pyle EH, Santoni GW, Nascimento HEM, Hutyra LR, Vieira S, Curran DJ, van Haren J, Saleska SR, Chow VY, Carmago PB, et al. 2008. Dynamics of carbon, biomass, and structure in two Amazonian forests. Journal of Geophysical Research 113:G00B08.

Read JM, Clark DB, Venticinque EM, Moreira MP. 2003. Application of merged 1-m and 4-m resolution satellite data to research and management in tropical forests. Journal of Applied Ecology 40:592–600.

Rice AH, Pyle EH, Saleska SR, Hutyra L, Camargo PB, Portilho K, Marques DF, Palace M, Keller M, Wofsy SC. 2004. Carbon balance and vegetation dynamics in an old-growth Amazonian forest. Ecological Applications 14:S55–S71.

Rich PM. 1989. A manual for analysis of hemispherical canopy photography (CANOPY PROGRAM). Los Alamos (NM): Los Alamos National Laboratory.

Runkle JR. 1981. Gap regeneration in some old-growth forests of the eastern United States. Ecology 62:1041–1051.

Shimabukuro YE, Smith JA. 1991. The least-squares mixing models to generate fraction images derived from remote sensing multispectral data. IEEE Transactions on Geoscience and Remote Sensing 29:16–20.

Shugart H. 1984. A theory of forest dynamics: the ecological implications of forest succession models. New York: Springer–Verlag.

Silver WL, Neff J, McGroddy M, Veldkamp E, Keller M, Cosme R. 2000. Effects of soil texture on belowground carbon and nutrient storage in a lowland Amazonian forest ecosystem. Ecosystems 3:193–209.

Taylor M. 2009. IKONOS planetary reflectance and mean solar exoatmospheric irradiance.

Team R. 2005. R: A language and environment for statistical computing, reference index version 2.2.1. R Foundation for Statistical Computing.

Toutin T. 2004. Review article: Geometric processing of remote sensing images: models, algorithms and methods. International Journal of Remote Sensing 25: 1893–1924.

Tucker CJ. 1979. Red and photographic infrared linear combinations for monitoring vegetation. Remote Sensing of the Environment 8:127–150.

Turner MG. 2010. Disturbance and landscape dynamics in a changing world. Ecology 91:2833–2849.

Uhl C, Clark K, Dezzeo N, Maquirino P. 1988. Vegetation dynamics in Amazon treefall gaps. Ecology 69:751–763.

van der Meer PJ, Bongers F. 1996. Formation and closure of canopy gaps in the rain forest at Nouragues, French Guiana. Vegetatio 126:167–179.

van der Meer PJ, Bongers F, Chatrou L, Riera B. 1994. Defining canopy gaps in a tropical rain-forest – Effects on gap size and turnover time. Acta Oecologica–International Journal of Ecology 15:701–714.

Welles JM, Norman JM. 1991. Instrument for indirect measurement of canopy architecture. Agronomy Journal 83:818–825.

Whitmore TC. 1989. Canopy gaps and the two major groups of forest trees. Ecology 70:536–538.

Young TP, Hubbell SP. 1991. Crown asymmetry, treefalls, and repeat disturbance of broad-leaved forest gaps. Ecology 72:1464–1471.

Supplemental Material

Gap formation and carbon cycling in the Brazilian Amazon: measurement using high-resolution optical remote sensing and studies in large forest plots

Fernando D.B. Espírito-Santo[1,2*], Michael M. Keller[1,3,4], Ernst Linder[5], Raimundo Cosme Oliveira Junior[6], Cleuton Pereira[7] and Cleber G. Oliveira[8]

[1] Institute for the Study of Earth, Oceans and Space (EOS), Morse Hall, Univ. of New Hampshire, Durham NH, US.
[2] Jet Propulsion Laboratory (JPL), Radar Science and Eng. Section, Pasadena, CA, US.
[3] USDA Forest Service, International Institute of Tropical Forestry, San Juan, Puerto Rico.
[4] EMBRAPA – CNPM, Campinas, SP, Brazil.
[5] Dept. of Mathematics and Statistics, Univ. of New Hampshire, Durham, NH, US.
[6] EMBRAPA Amazônia Oriental, Santarém, PA, Brazil.
[7] Santarém, PA, Brazil.
[8] Remote Sensing Division, National Inst. Space Research (INPE), São José dos Campos, SP, Brazil.

*correspondence: Fernando D.B. Espírito-Santo, email: f.delbon@gmail.com

Geostatistical analysis of light environments

We interpolated all collections of CO and LAI from LAI-2000 PCA of the two large plots using Kriging (Cressie, 1993). We used a semivariogram $\gamma(h)$ to calculate the kriging weights of CO and LAI ground collections, given by:

$$\gamma(h) = \frac{1}{2} Var\left[z(s_i + h) - z(s_i)\right] \tag{1}$$

where $\gamma(h)$ is a estimated semivariance value given a lag (h) considering a variable with the spatial location $z(s_i)$ and its neighboring at distance $s_i + h$. All the geostatistical analyses were executed using geoR (Ribeiro and Diggle, 2001) and Fields (Fields Development Team, 2006) packages of R language (R Development Core Team, 2005).

We fit several theoretical semivariogram models (linear, spherical, exponential, Gaussian and power) using the weighted least squares method and we selected the model with smallest RMSE and the best correlation. Three parameters were used to fit the semivariogram: (1) range equal to the maximum distance of spatial dependence of a variable; (2) sill a variance related to the spatial structure of the data; and (3) nugget equal to the residual variation at the shortest sampling interval. Finally, we used the following ordinary kriging estimator (Z) of a number of measurements of CO and LAI (z_i) and its corresponding weightings (w_i) to predict the spatial distribution of CO over the sample areas:

$$Z(x, y) = \sum_{i=1}^{n} w_i z_i \tag{2}$$

Considering the skewed frequency distribution of DIFN, we applied a square root transformation on the raw data of CO in both large forest inventory plots. No transformation was applied to LAI because the square root transformation did not markedly affect its skewness (see Sup. Material, S3-4).

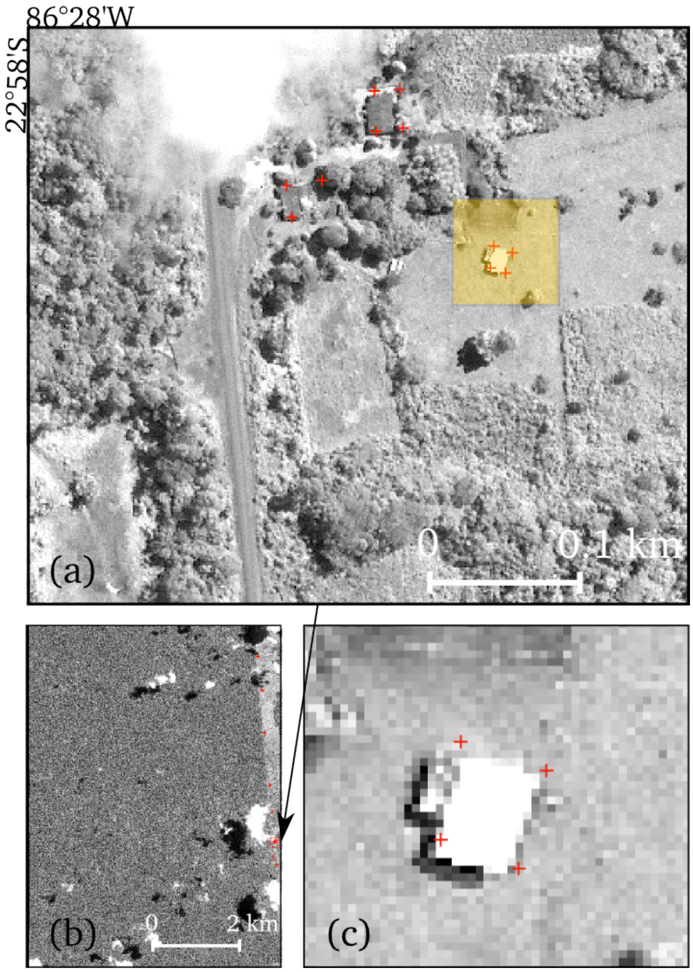

S1. GPS ground validation (red crosses) used in the orthorectification of the IKONOS-2 image. Civil construction features (a) were used as targets for GPS collections (b). House roofs (c) were used only for a general check of the ground validation but not for the ortorectification process considering the vertical difference between ground true data and off-nadir satellite angle.

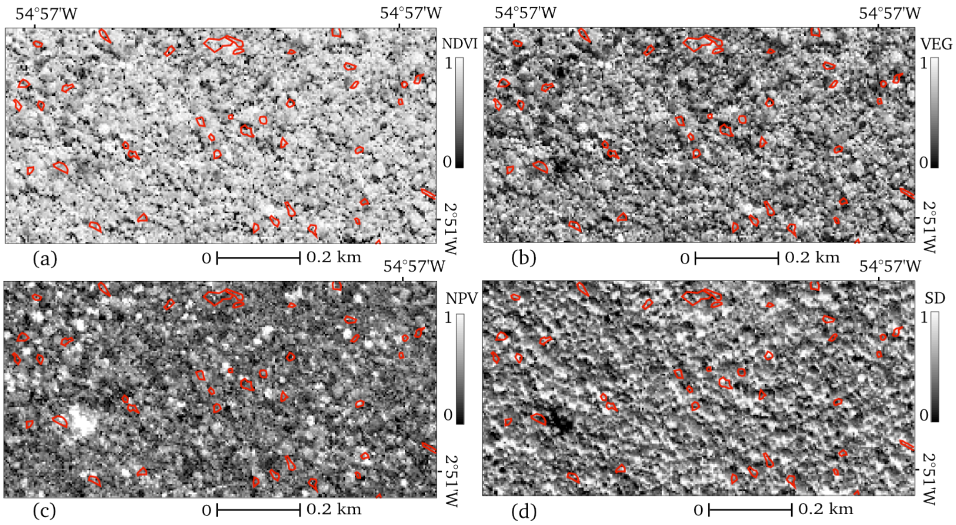

S2. IKONOS-2 image processing of 53 ha plot at Tapajós National Forest (Brazil). Normalized Difference Vegetation Index NDVI (a) and unmixing fraction images of green vegetation GV (b), non-photosynthetic vegetation NPV (c) and shade SD (d). Ground gaps (n=41) are overlaid in red.

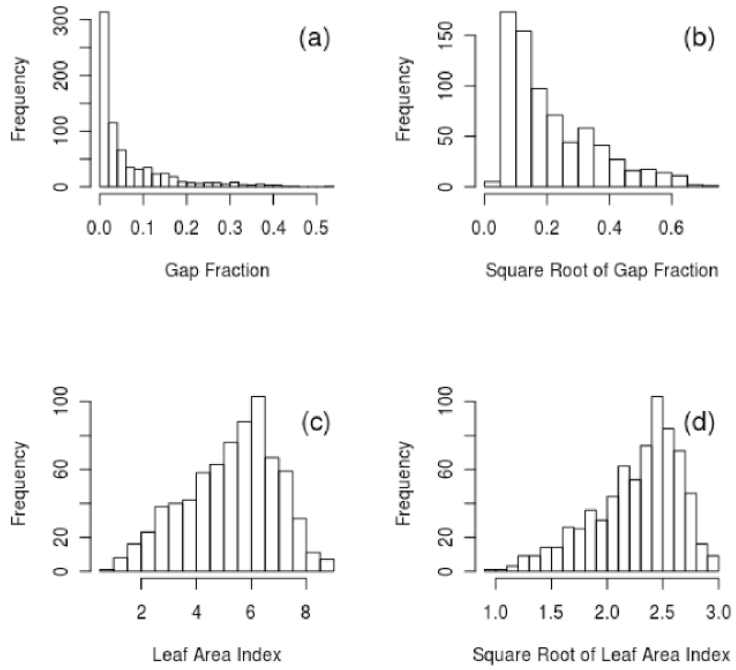

S3. Frequencies distribution of ground collection of LAI-2000 PCA in the 114 ha plot (n=731). Positive skewed frequency distribution of diffuse non-interceptance (DIFN) light or canopy openness (CO) (a). Square root transformation of CO to reduce the skewed data distribution (b). Negative skewed data distribution of LAI (c) and its square root transformation (d).

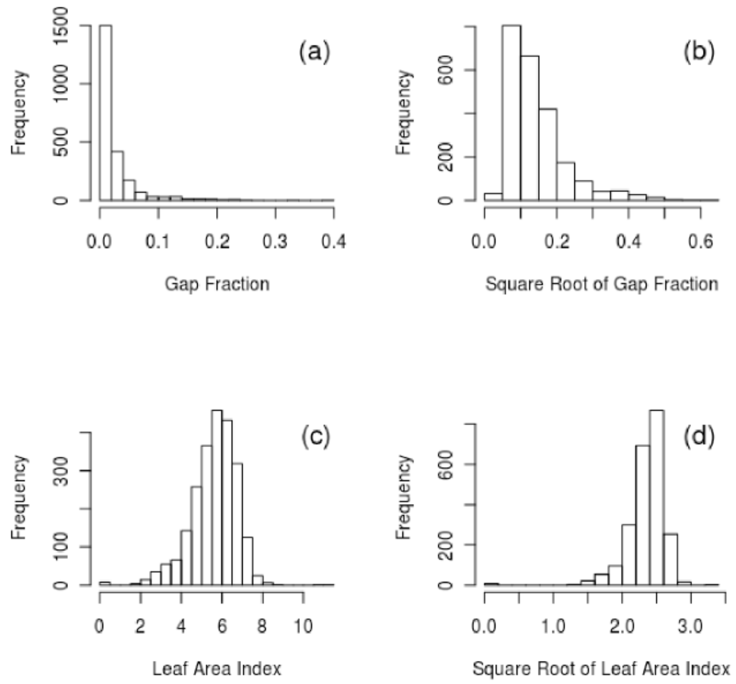

S4. Frequencies distribution of ground collection of LAI-2000 PCA in the 53 ha plot (n=2315). Positive skewed frequency distribution of diffuse non-interceptance (DIFN) light or canopy openness (CO) (a). Square root transformation of CO to reduce the skewed data distribution (b). Negative skewed data distribution of LAI (c) and its square root transformation (d).

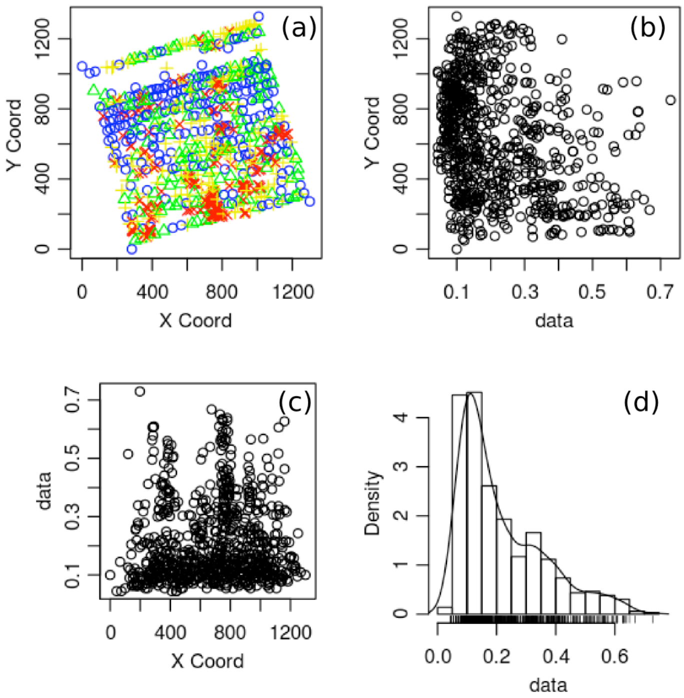

S5. Spatial distribution of canopy openness (square root of CO) (n=731) in the 114 ha plot (a), Colors signify CO ranges: 0.01-0.2 (blue), 0.21-0.3 (green), 0.31-0.4 (yellow) and > 0.41 (red). Scatter plot between CO and spatial coordinates Y (b) and X (c) and frequency distribution of gap fraction data (d).

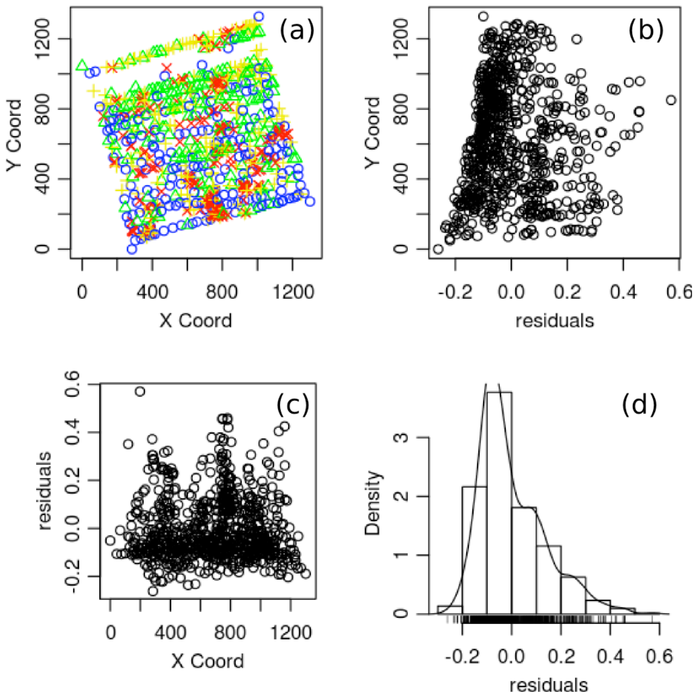

S6. Spatial distribution of canopy openness (square root of CO) (n=731) in the 114 ha plot (a), Colors signify CO ranges: 0.01-0.2 (blue), 0.21-0.3 (green), 0.31-0.4 (yellow) and > 0.41 (red). Scatter plot between CO and removed spatial trends of the coordinates Y (b) and X (c) and frequency distribution of CO residuals (d). The global spatial trend was removed from the original data (square root of CO) by polynomial linear model (Spatial trend = $X + Y + Y^2$) where the regression between the two variable reveled a trend of $r^2 = 0.10$ (F-statistic=28.08, 729 DF and $p<2.2e-16$). Coefficients are: 1.505e-01 (Intercept), 3.175e-06 (X), -2.187e-04 (Y) and 1.036e-07 (Y^2).

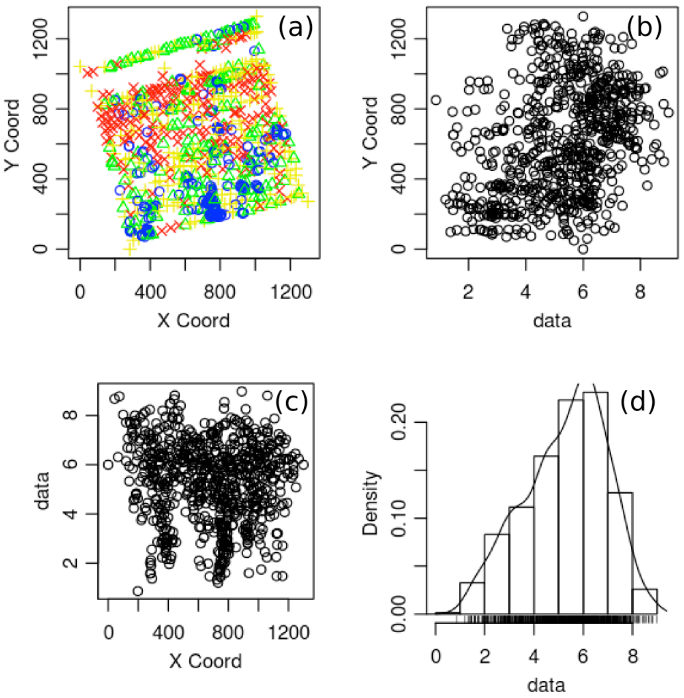

S7. Spatial distribution of leaf area index (LAI) (n=731) in the 114 ha plot (a). Colors mean LAI ranges: 0.1-3 (blue), 3.1-5 (green), 5.1-7 (yellow) and > 7.1 (red). Scatter plot between LAI and spatial coordinates Y (b) and X (c) and frequency distribution of LAI (d).

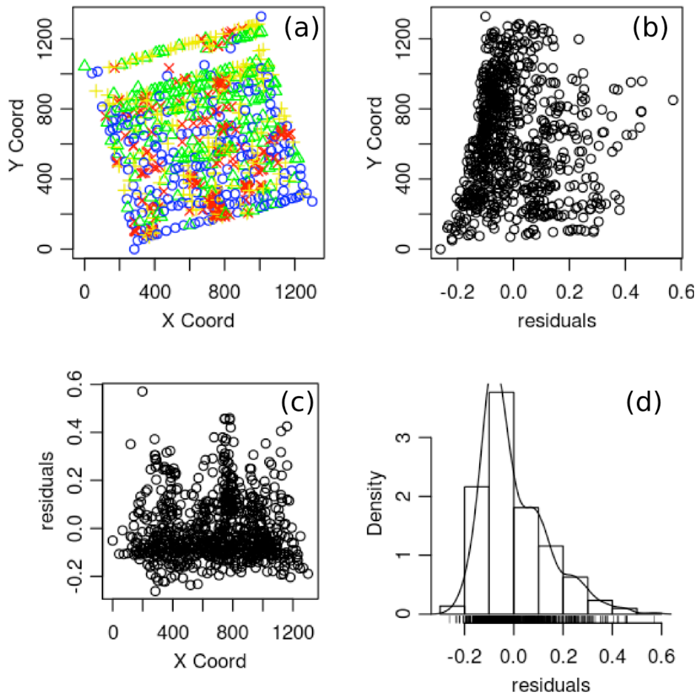

S8. Spatial distribution of LAI (n=731) in the 114 ha plot (a). Colors mean LAI ranges: 0.1-3 (blue), 3.1-5 (green), 5.1-7 (yellow) and > 7.1 (red). Scatter plot between LAI and removed spatial trends of the coordinates Y (b) and X (c) and frequency distribution of LAI residuals (d). The global spatial trend was removed from the original data (leaf area index) by polynomial linear model (Spatial trend = X + Y + Y^2) where the regression between the two variable revealed a trend with $r^2 = 0.17$. (F-statistic=52.49, 729 DF and $p<2.2e-16$). Coefficients are: 2.984 (Intercept), -4.031e-04 (X), 5.086e-03 (Y) and -2.676e-06 (Y^2).

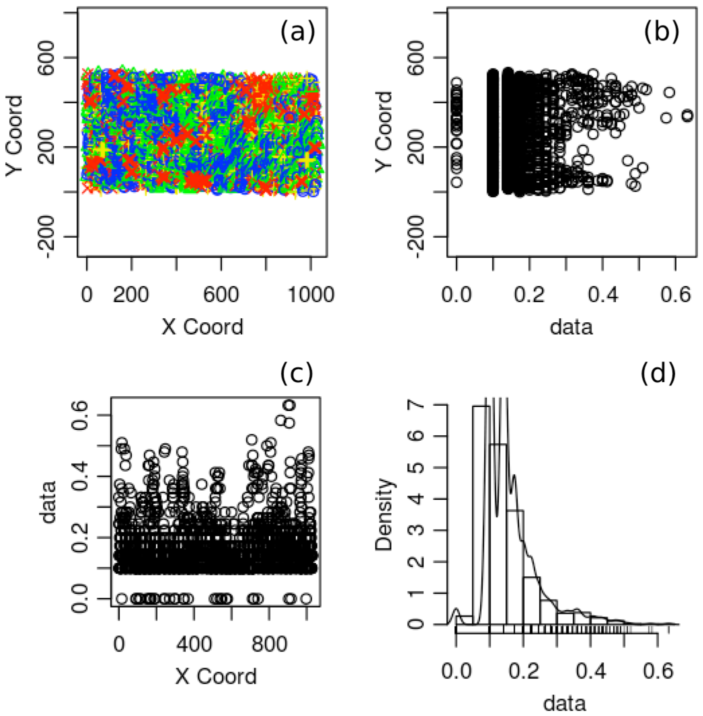

S9. Spatial distribution of canopy openness (square root of CO) (n=2315) in the 53 ha plot (a), Colors mean CO ranges: 0.01-0.15 (blue), 0.16-0.2 (green), 0.21-0.3 (yellow) and > 0.31 (red). Scatter plot between gap fraction and spatial coordinates Y (b) and X (c) and frequency distribution of gap fraction data (d).

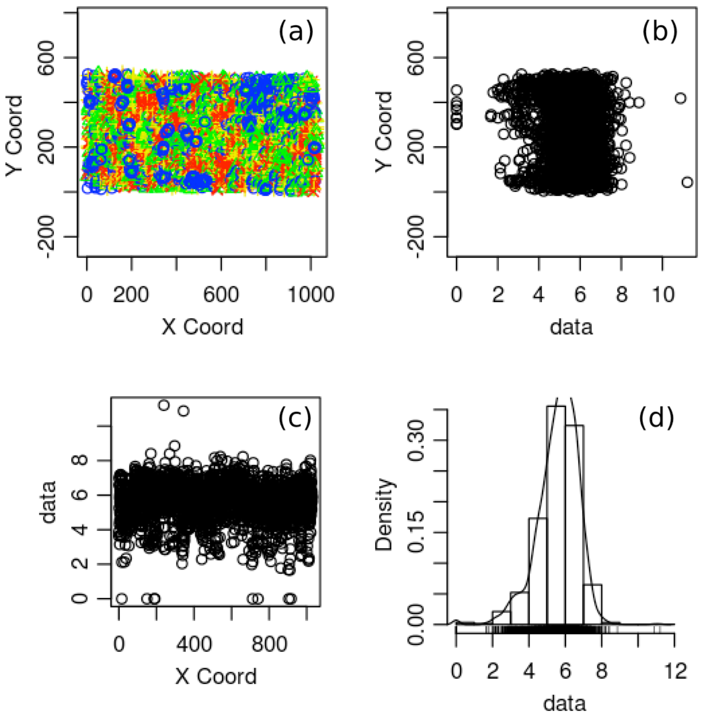

S10. Spatial distribution of LAI (n=2315) in the 53 ha plot (a). Colors mean CO ranges: 0.1-3 (blue), 3.1-5 (green), 5.1-7 (yellow) and > 7.1 (red). Scatter plot between LAI and spatial coordinates Y (b) and X (c) and frequency distribution of leaf area index data (d).

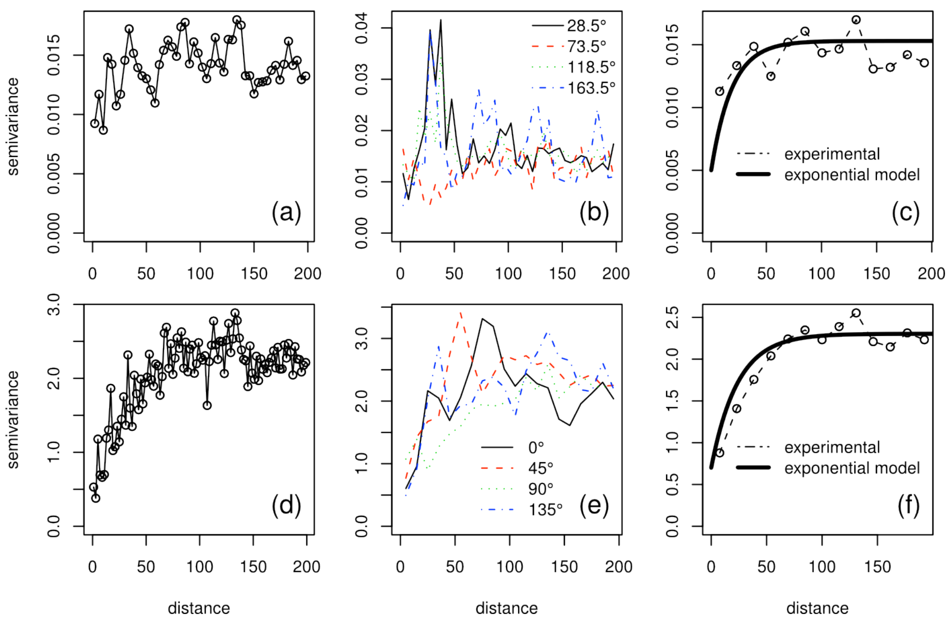

S11. Geostatistical analysis of ground remote sensing collections for the 114 ha plot. Semivariograms of canopy openness (square root of CO): unidirectional (a), multi-directional (b) and modeled exponential semivariogram (c). Experimental semivariograms for LAI: unidirectional (d), multi-directional (e) and modeled exponential semivariogram (f).

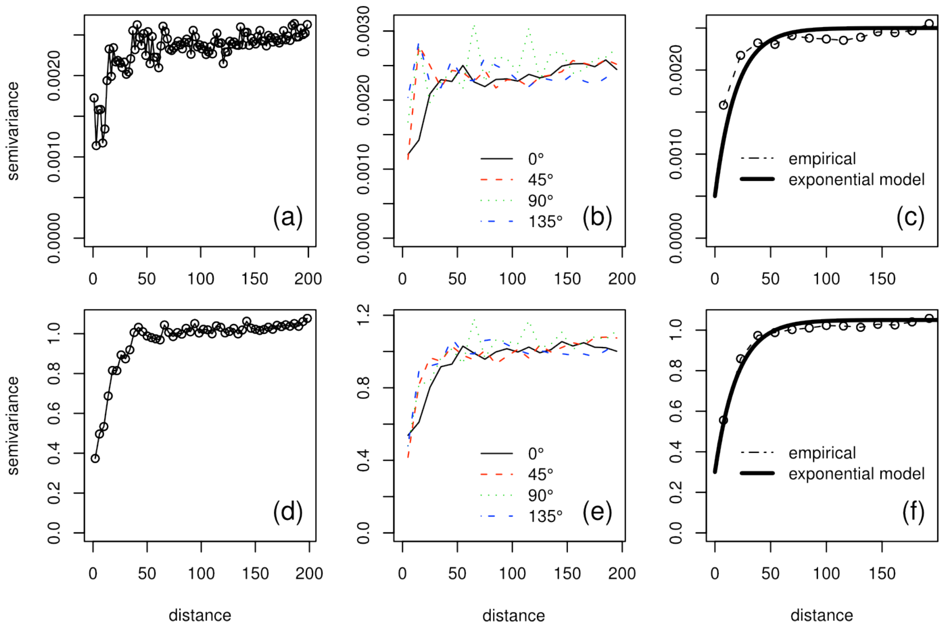

S12. Geostatistical analysis of ground remote sensing collections of 53 ha plot. Semivariograms of canopy openness (square root of CO): unidirectional (a), multi-directional (b) and modeled exponential semivariogram (c). Experimental semivariograms for LAI: unidirectional (d), multi-directional (e) and modeled exponential semivariogram (f).

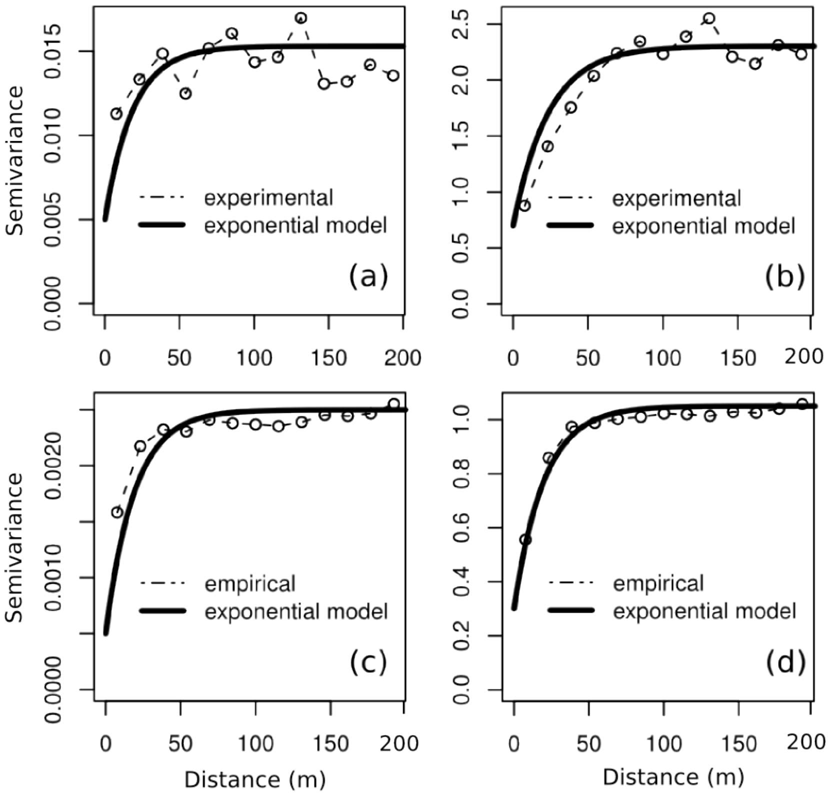

S13. Empirical and fitted exponential semivariogram models for canopy openness - CO (a) and leaf area index - LAI (b) for the 114 ha plot (n=731). For the 53 ha plot (n=2315) a fitted exponential semivariogram models was also applied for CO (c) and LAI (d). Kriging parameters used to interpolate CO and LAI in 114 ha plot were, respectively: direction (isotropy in both), nugget (0.0055 and 0.4586), sill (0.0103 and 1.603) and range (56.1 m and 71.16 m). For the 53 ha kriging plots of CO and LAI we used: direction (isotropy in both), nugget (0.0026 and 0.3922), sill (0.0028 and 0.7507) and range (57.26 m and 60.26 m). A square root transformation was applied for the raw data of CO or (DIFN) to reduce its skewed frequency distribution in both plots.

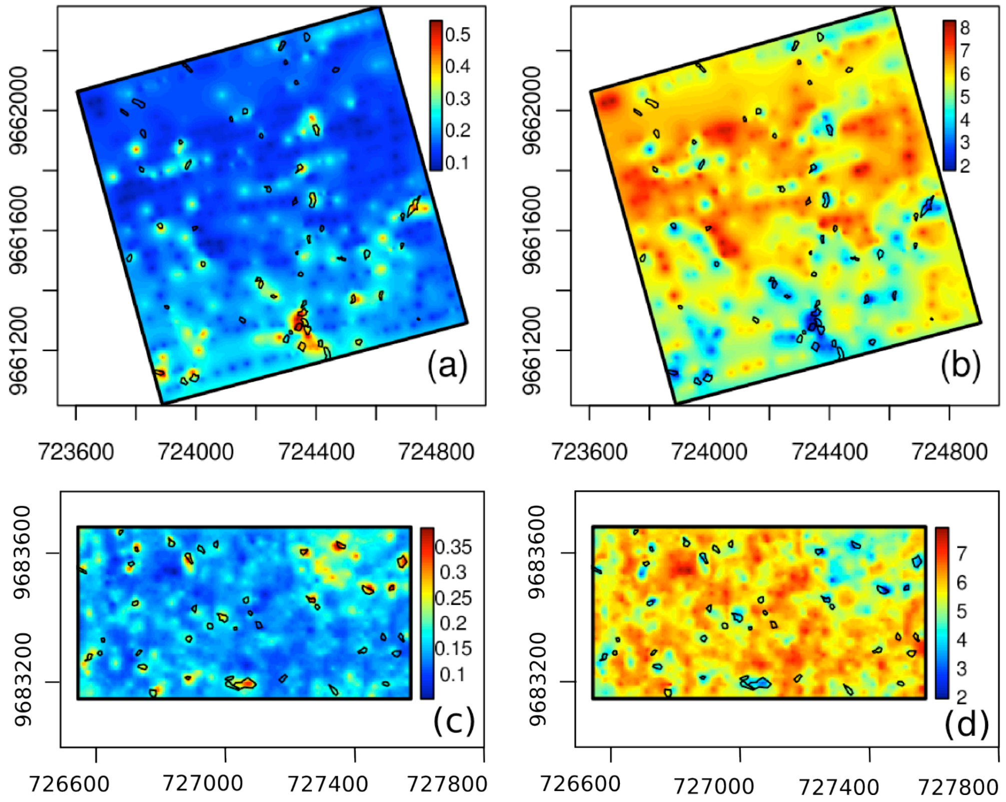

S14. Interpolated canopy openness (square root of CO) (a) and leaf area index (LAI) (b) in the 114 ha plot (n=731) using the exponential semivariogram model (c.f. Figure S11) and canopy openness (square root of CO) (c) and leaf area index (LAI) (d) in the 53 ha forest inventory plot (n=2315) (c.f. Figure S12). Gap areas (black polygons) are present in areas of high fraction of canopy openness for both plots (*a* and *c*). The leaf area index drops considerably (2 to 4) around of tree fall gaps (*b* and *d*).

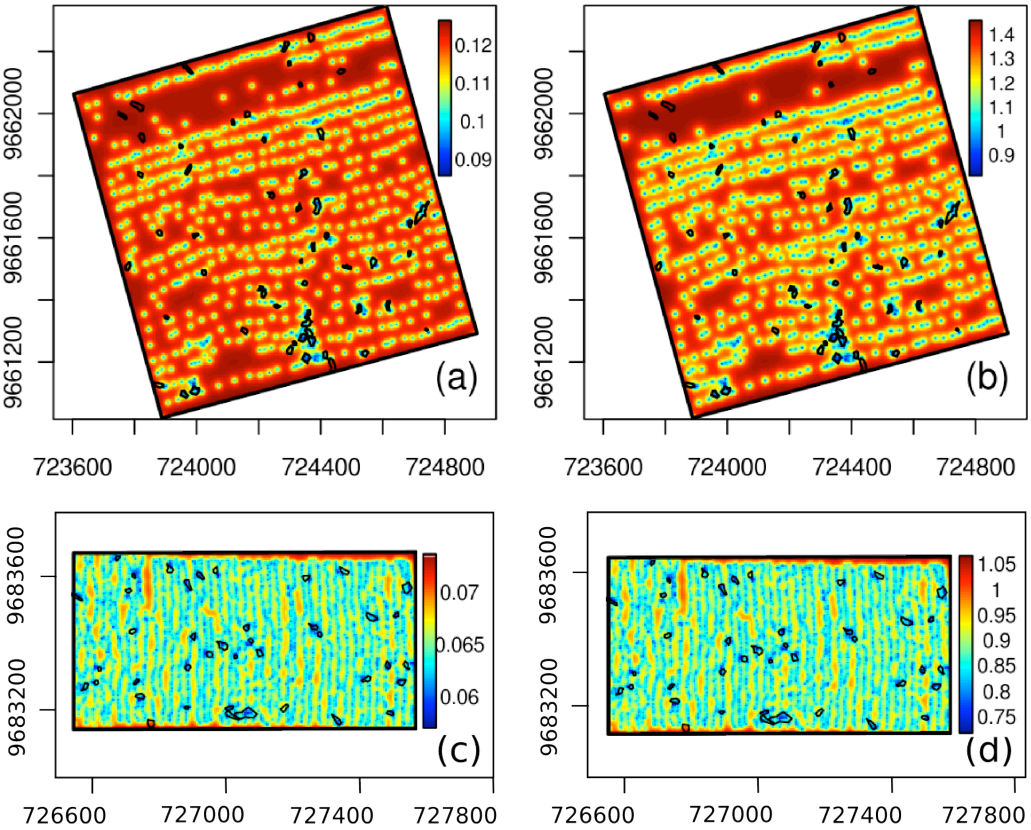

S15. Interpolation uncertainty (standard error) of canopy openness (a) and LAI (b) of the 114 ha plot (n=731) and canopy openness (c) and LAI (d) for the 53 ha plot (n=2315).

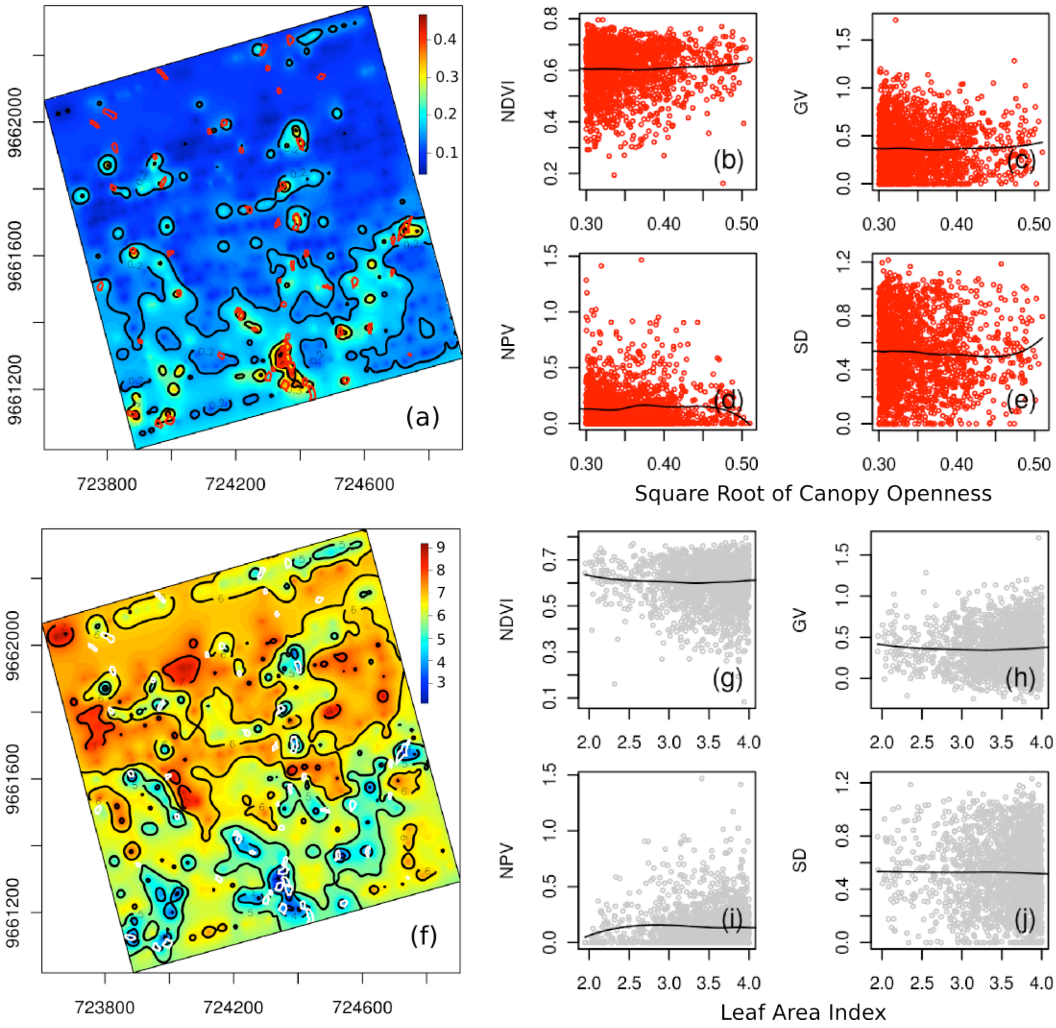

S16. Contour map of canopy openness (square root of CO) in the 114 ha forest plot showing high CO ≥ 0.3 (yellow) in areas of tree fall gaps (red polygons). Scatter plots where square root CO ≥ 0.3 or 0.09 CO and remote sensing products (n=1817 pixels of 4 m): NDVI (b), green vegetation (c), nonphotosynthetic vegetation (d) and shade (e). Contour map of LAI showing low LAI ≤ 4 (dark blue grid spots) in regions of tree-fall gaps (white polygons). Scatter plots for LAI ≤ 4 and remote sensing products (n=1869 pixels of 4 m): NDVI (g), green vegetation (h), nonphotosynthetic vegetation (i) and shade (j). Fitted curves for all ground measurements and remote sensing products are not significant (p<0.05).

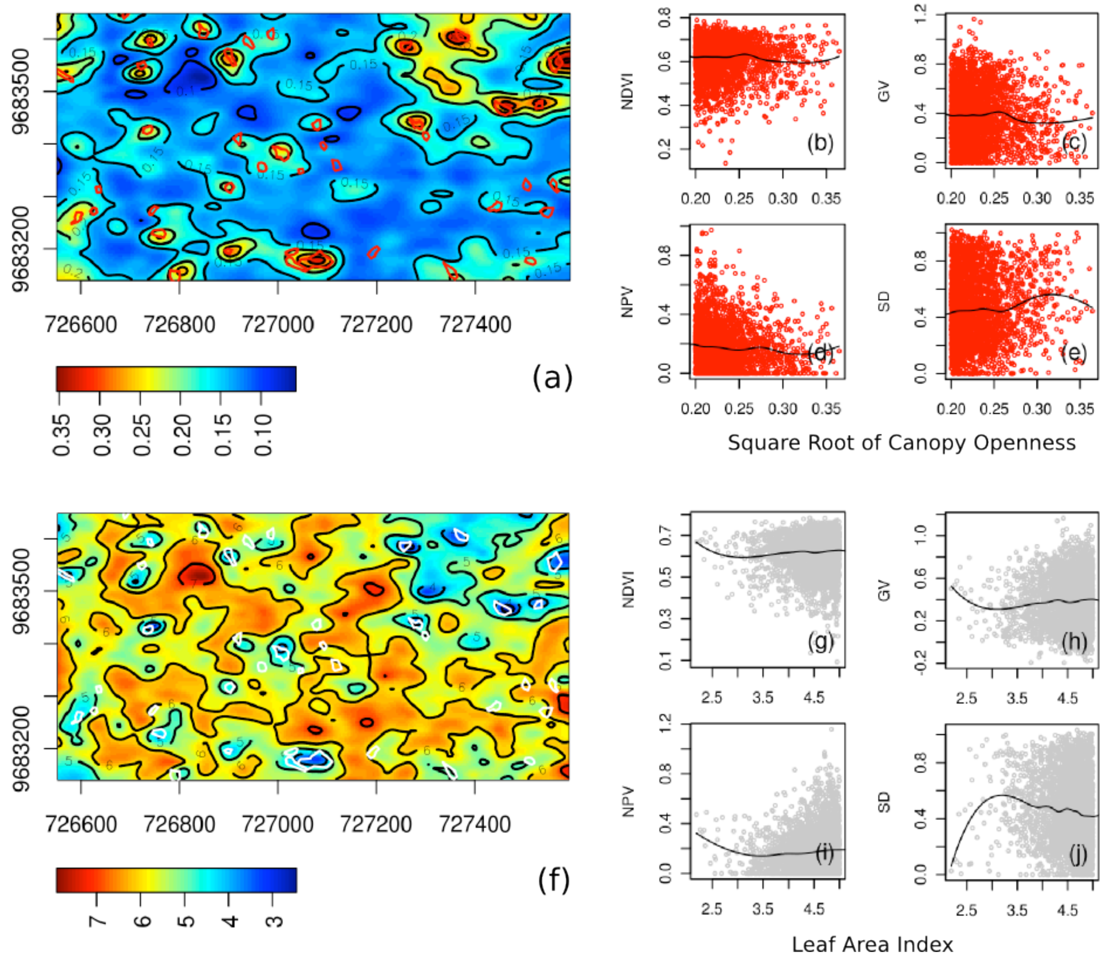

S17. Contour map of canopy openness (square root of CO) in the 53 ha forest area showing high CO ≥ 0.23 (yellow grid spots) in areas of tree fall gaps (red polygons). Scatter plots for values of square root of CO ≥ 0.23 or CO ≥ 0.0625 and remote sensing products (n=1102 pixels of 4 m): NDVI (b), green vegetation (c), nonphotosynthetic vegetation (d) and shade (e). Contour map of LAI showing low LAI ≤ 4 (light blue grid spots) in regions of tree-fall gaps (white polygons). Scatter plots for data where LAI ≤ 5 and remote sensing products (n=3764 pixels of 4 m): NDVI (g), green vegetation (h), nonphotosynthetic vegetation (i) and shade (j). Fitted curves for all ground measurements and remote sensing products are not significant (p<0.05).

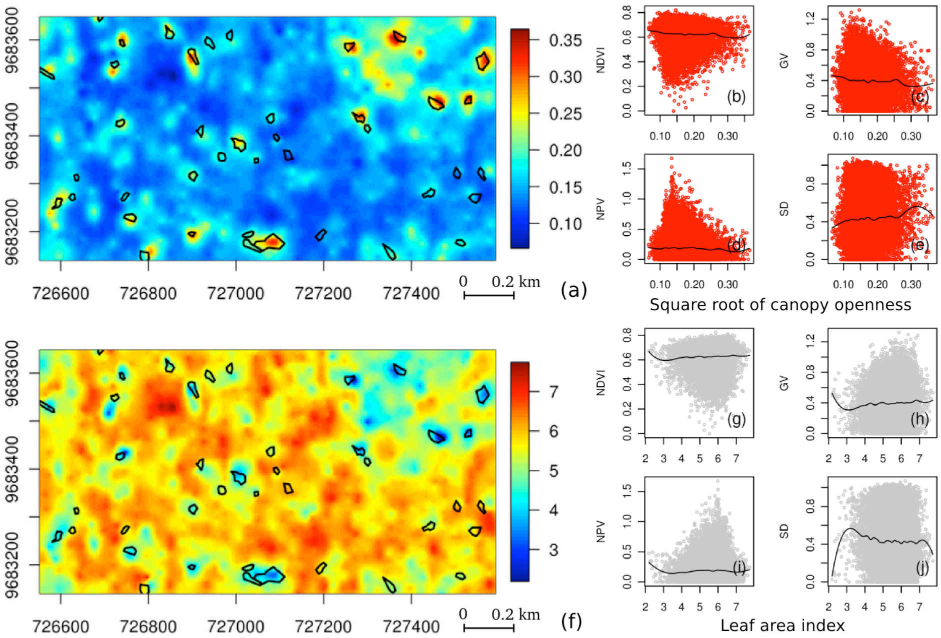

S18. Interpolated ground collections (n=2315) of canopy openness (square root of CO) (a) and leaf area index (LAI) (f) in 53 ha forest area (4 meter grid plot) using kriging with an exponential semivariogram model. Gaps (black polygons) are present in areas of high opened sky (a) and low leaf area index (f). Scatter plots of canopy openness grid and remote sensing products (4 m spatial resolution): NDVI (b), green vegetation GV (c), non-photosynthetic vegetation NPV (d) and shade SD (e). For LAI grid plot the scatter plots with the same remote sensing products are: NDVI (g), green vegetation (h), non-photosynthetic vegetation (i) and shade (j).

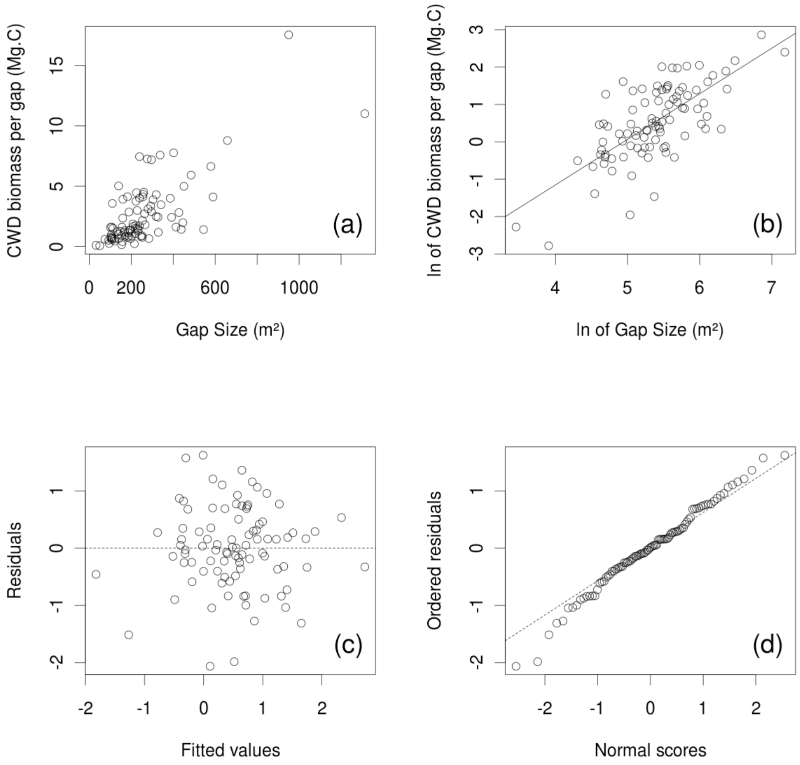

S19. Coarse woody debris CWD (Mg C) in gaps versus gap size area (m^2) and coarse wood debris in gaps of two large plots (167 ha and n=92 gaps) (a). Log-log graph of gap area and CWD (b). Residuals of the linear regression (c) and its theoretical normalized quantiles (d). Pearson correlation r=0.72, fitted adjusted regression model R^2=0.53 and p-value<0.01. Intercept and slope are respectively, -0.1551 and 0.0108.

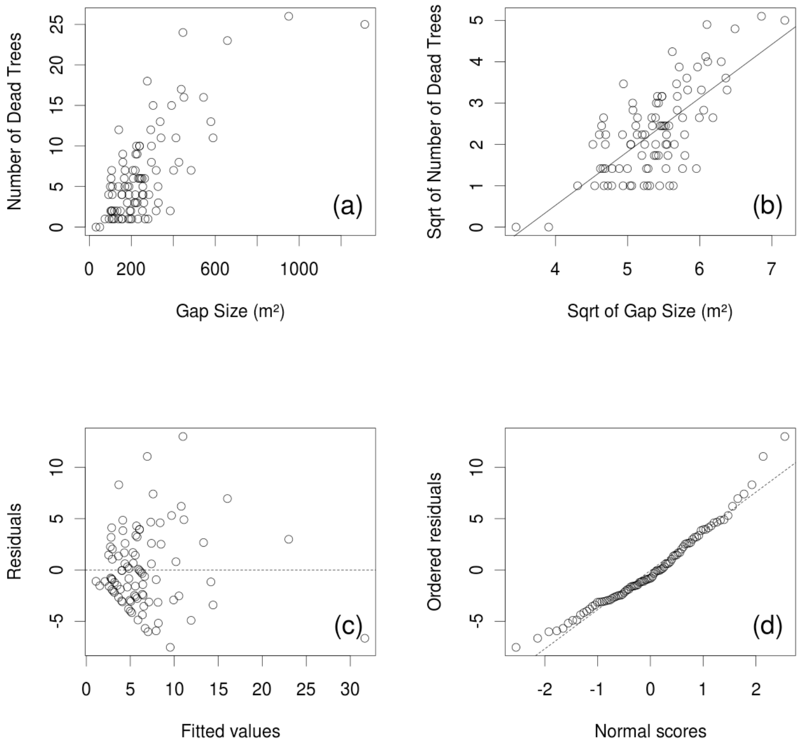

S20. Plot of the number of dead trees versus gap size area (m^2) in two large plots (167 ha and n=92 gaps) (a). Square root transformation graph of gap area and number of dead trees (b). Residuals of the linear regression (c) and its theoretical normalized quantiles (d). Pearson correlation r=0.74, fitted adjusted regression model R^2=0.56 and p-value < 0.01. Intercept and slope are respectively, 0.3485 and 0.0238.